

Network Modelling of Asynchronous Change-Points in Multivariate Time Series

Carson McKee¹ and Maria Kalli²

¹*Department of Mathematics, King's College London, carson.mckee@kcl.ac.uk*

²*Department of Mathematics, King's College London, maria.kalli@kcl.ac.uk*

Abstract

This article introduces a novel Bayesian method for asynchronous change-point detection in multivariate time series. This method allows for change-points to occur earlier in some series (leading series) followed, after a short delay, by change-points in some other series (lagging series). Such dynamic dependence structure is common in fields such as seismology and neurology where a latent event such as an earthquake or seizure causes certain sensors to register change-points before others. We model these lead-lag dependencies via a latent directed graph and provide a hierarchical prior for learning the graph's structure and parameters. Posterior inference is made tractable by modifying particle MCMC methods designed for univariate change-point problems. We apply our method to both simulated and real datasets from the fields of seismology and neurology. In the simulated data, we find that our method outperforms competing Bayesian methods in settings where the change-point locations are dependent across series. In the real data applications we show that our model can also uncover interpretable network structure.

Keywords: Multivariate, Change-Point, Asynchronous, MCMC, Particle Gibbs, Network, Time Series

1 Introduction

Change-point models are employed to infer the locations of abrupt changes in the distribution of a time series. These models assume that some combination of the distribution's parameters shift at the change locations. Change-point analysis plays a critical role in modelling non-stationary systems, where structural changes arise from external shocks or internal dynamics. A model that correctly detects such changes leads to enhanced predictive performance and supports more reliable decision-making by accounting for shifts in underlying processes. The accurate detection of change-points also offers insight into the causal factors driving the behaviour of a dynamic system. Change-point models have been applied in many fields such as medicine (Liu et al., 2017; Kass-Hout et al., 2012), finance and economics (Chib, 1998; Bauwens et al., 2017; Maheu and Song, 2018) and hydrology (Alaya et al., 2020).

When analysing multiple time series, it is common to observe patterns such as simultaneous changes or short delays in changes across subsets of dependent series. This is often due to a common latent process driving the change-points across different series. A particularly important pattern, observed in many applications is the *lead-lag* relationship, where *leading* series tend to experience change-points shortly before their corresponding *lagging* series. Identifying lead-lag relationships is important both for prediction — since a change in a leading series may signal an imminent change in a lagging series — and for inference, by providing insight into the latent processes connecting the series.

In this article we present a novel Bayesian method for modelling multivariate change-points in a variety of settings. Our approach encourages change-points to appear earlier in some (leading) series, followed shortly after by change-points in other (lagging) series. To encode these lead-lag relationships we use a latent directed graph where vertices represent the series and a directed edge from one vertex/series to another indicates that one series leads the other. The strength of the lead-lag relationships and the delays between change-points are controlled via a set of edge parameters. We assume that both the edge set and edge parameters are unknown and will be inferred in addition to the

change-point locations. To perform posterior inference we extend the efficient particle Gibbs sampler of Whiteley et al. (2011) used in univariate change-point models to the multivariate setting.

Although lead-lag relationships arise in many fields, our work is motivated by two specific examples. The first concerns the detection of seismic events using observations from multiple ground motion sensors. In this setting, an event such as an earthquake induces abrupt changes in the amplitude and frequency content of the sensor signals as the primary (P) and secondary (S) waves arrive. Sensors located closer to the fault line typically register change-points earlier than those further away, giving rise to a lead-lag relationship across the multiple series. Here, the lead-lag relationships are driven by spatial proximity, and modelling them may improve detection accuracy of weaker events at more distant sensors.

The other motivating example is the detection of seizures using electroencephalogram (EEG) signals. EEG analysis involves recording the brain’s electrical activity over time using electrodes placed on the scalp. The occurrence of a seizure results in sudden changes in the amplitude and rhythmic patterns of the EEG signals. These changes are initially detected in the electrodes closest to the seizure onset zone and typically propagate to nearby electrodes shortly thereafter as the seizure spreads to other regions of the brain. In this context, lead-lag relationships are driven by the seizure’s dynamics and propagation pathway. Inferring this pathway is crucial for understanding the brain’s network structure and for developing personalized treatment strategies aimed at preventing the seizure from spreading.

The literature on performing change-point detection in the univariate setting is quite large. Frequentist approaches date back to Page (1954) and generally involve minimising cost functions or recursively applying tests to detect multiple changes. Recent advances in this area include the Pruned Exact Liner Time (PELT) method (Killick et al., 2012) and wild binary segmentation (Fryzlewicz, 2014). For a selective review of these techniques, see for example Truong et al. (2020).

Univariate Bayesian methods can be traced back to Chernoff and Zacks (1964) and require a prior distribution for the change-point locations. These models typically assume the change-points follow a Markov chain, differing in how they define the transitions and whether the number of changes is known or unknown. When the number of changes is known, we may use a finite state hidden Markov model (HMM), see for example Chib (1996). For an unknown number of changes, we may compare various finite state models with Bayes factors (Chib, 1998), however, this quickly becomes intractable when comparing many models. An alternative solution is to use the infinite hidden Markov model of Beal et al. (2002), a nonparametric extension of Chib (1996) which allows for a countably infinite number of states.

An alternative and widely used approach to modelling an unknown number of change-points is to use Product Partition Models (PPMs) (Hartigan, 1990), which generalise several previous methods, such as that of Yao (1984). These models specify a distribution over the random partition induced by the change-points and can also be formulated as a Markov chain (Barry and Hartigan, 1992). However, unlike HMMs which may re-enter previous states, a change-point under a PPM always introduces a completely new state. Recent work employing PPMs include (Nyamundanda et al., 2015; García and and, 2019; Corradin et al., 2022). While conceptually simple to specify, Bayesian methods often require Monte Carlo sampling in order to obtain posterior estimates, see for example Fearnhead (2006).

Less attention has been given to the multivariate setting where changes may affect subsets of the series at synchronised or nearly synchronised times. Motivated by applications in genomics, much of the frequentist literature focuses on detecting synchronized changes in the mean of Gaussian random variables. When changes are assumed to affect all series simultaneously, Zhang et al. (2010) propose a scanning procedure which sums the chi-squared statistics across each series and show that their method leads to improved detection accuracy. A more general approach was introduced by Siegmund et al. (2011) which includes the method of Zhang et al. (2010) as a special case.

When synchronised changes are observed on only a small subset of the series, Jeng et al. (2013) proposed the Proportion Adaptive Segment Selection (PASS) procedure, which automatically adapts to the unknown number of series which experience synchronised change-points. An alternative method is proposed by Wang and Samworth (2018) who first produce a sparse projection of the series before applying the cumulative sum (CUSUM) test to detect a single change in the resulting series. Multiple change-points can then be handled by combining this with the binary segmentation method of Fryzlewicz (2014).

Similar to the frequentist literature, most existing Bayesian methods are designed for analysing synchronised change-points and build upon existing univariate methods. For example, Fan and Mackey

(2017) proposed an empirical Bayes method, such that for each fixed time, the prior change-point probabilities are the same across all series, and can vary with time. A fully Bayesian method, motivated by the univariate PPM approach (Barry and Hartigan, 1992), was proposed by Quinlan et al. (2024). This method also encourages synchronized changes by specifying a joint distribution for the vector of prior change-point probabilities for each fixed time. A related problem was considered by Bardwell and Fearnhead (2017) who proposed the Bayesian Abnormal Segments Detector (BARD) method. This method models the change-point locations with a Markov chain and attempts to identify segments where a subset of the series differs from some baseline behaviour. The three methods of Fan and Mackey (2017); Bardwell and Fearnhead (2017); Quinlan et al. (2024) encourage subsets of the series to exhibit synchronised changes *a priori*, but ignore any dependence which may arise when change-points occur asynchronously. Similarly, they provide no method for inferring which subsets of the series exhibit dependence (other than manually inspecting the posterior change-point probabilities).

A Bayesian method that allows for both synchronous and asynchronous dependence in the change locations was proposed by Hallgren et al. (2024) who assumed that the series are connected via a known weighted undirected graph. Under this model, series which are connected on the graph are more likely to experience changes at similar, but not necessarily synchronised times. While this method allows for asynchronous dependence, it does not account for lead-lag relationships and requires us to supply a graph linking the series which, in general, may not be known.

Our approach to modelling multivariate change-points is similar to Hallgren et al. (2024). We too assume that the series are connected via a latent weighted graph. However, unlike the approach of Hallgren et al. (2024), we do not assume the graph is known *a priori* and we provide a hierarchical prior to enable learning on the graph parameters. Since we are interested in lead-lag relationships we use a directed graph to account for directed dependence.

The remainder of this article is organised as follows, Section 2 introduces the proposed model and discusses its properties. In Section 3 we describe a novel blocked particle Gibbs scheme to obtain posterior samples. In Section 4 we demonstrate our methods through a comparative simulation study and two real data examples before concluding with a discussion in Section 5.

2 The Model

In this section we introduce our modelling approach, which we refer to as Network Change-Point (NetCP) model, and related notation. We consider a multivariate time series of dimension d , observed at times $t = 1, \dots, T$. Let $\mathbf{Y}_t = (Y_{1,t}, \dots, Y_{d,t})'$ denote the vector of observations at time t and $\mathbf{Y} = (\mathbf{Y}_1, \dots, \mathbf{Y}_T)$ be the $(d \times T)$ matrix which holds the observations. Conditional on a set of change-point locations, the data in each series is partitioned into non-overlapping segments such that the change-points correspond to the segment end-points. We use the notation $\mathbf{Y}_{j,s:t} = (Y_{j,s+1}, \dots, Y_{j,t})$ to denote the segment of observations in series j between change-points s and t .

We model the change-point locations with a multivariate hidden state process. Each observation $Y_{j,t}$ is assigned a hidden state $X_{j,t}$, which denotes the time of the most recent change-point in series j before time t . Our prior distribution over the hidden states \mathbf{X} is parameterised according to a latent directed graph linking the pairs of series that are dependent. We focus on posterior inference for both the hidden states and the graph parameters.

2.1 Likelihood Model

We first describe the likelihood model conditional on the hidden state process. Recall that $X_{j,t}$ denotes the time of the most recent change-point in series j prior to time t , then event $X_{j,t} = t - 1$ indicates that a change-point occurred at time $t - 1$. So, conditional on $\mathbf{X} = \mathbf{x}$, the set of change-point locations in series j is given by

$$\tau_j = \{i \in \{0, \dots, T - 1\} : x_{j,i+1} = i\} \cup \{T\}$$

The change-points partition the observations in each series j into $|\tau_j| - 1$ segments, where the k^{th} segment is given by $\tau_{j,k} : \tau_{j,k+1} = \{\tau_{j,k} + 1, \dots, \tau_{j,k+1}\}$. We assume that the observations in the k^{th} segment have density $f_j(\mathbf{y}_{j,\tau_{j,k}:\tau_{j,k+1}} | \theta_{j,k})$ where the parameter $\theta_{j,k} \in \Theta$ is segment specific and is drawn independently from the density $f_j(\cdot)$.

For computational reasons, (see Barry and Hartigan, 1993; Fearnhead, 2006), the densities $f_j(\cdot | \theta)$ and $f_j(\cdot)$ commonly chosen to be conjugate, enabling us to analytically marginalise over the segment

specific parameters:

$$f_j(\mathbf{y}_{j,s:t}) = \int_{\Theta} f_j(\mathbf{y}_{j,s:t}|\theta) f_j(\theta) d\theta \quad (1)$$

The resulting density $f_j(\mathbf{y}_{j,s:t})$ is referred to as the marginal segment density. Throughout this paper we will assume that (1) is available analytically, or can be approximated numerically in low dimensions. Under these assumptions, the joint likelihood may be expressed as

$$f(\mathbf{y}|\mathbf{x}) = \prod_{j=1}^d f_j(\mathbf{y}_{j,0:T}|\mathbf{x}_{j,0:T}) \quad (2)$$

$$= \prod_{j=1}^d \prod_{t=1}^T f_j(y_{j,t}|x_{j,t}, \mathbf{y}_{j,0:t-1}) \quad (3)$$

where

$$f_j(y_{j,t}|x_{j,t}, \mathbf{y}_{j,0:t-1}) = \frac{f_j(\mathbf{y}_{j,x_{j,t}:t})}{f_j(\mathbf{y}_{j,x_{j,t}:t-1})} \quad (4)$$

can be computed from the marginal segment densities given in Equation (1). The likelihood structure given in Equations (1) - (4) has been widely used in both the univariate and multivariate change-point literature (Barry and Hartigan, 1993; Fan and Mackey, 2017; Hallgren et al., 2024).

The specific choice of $f_j(\cdot|\theta)$ and $f_j(\cdot)$ depends on the application area. In Section 4 we apply our model to seismology and EEG data, where the focus is detecting changes in the variability and/or autocorrelation structure of each signal. To do this, this we employ an independent autoregressive model for the data within each segment of each series, such that both the lag coefficients and variance can vary across segments. In particular, we assume the segment specific parameters are $\theta := (\boldsymbol{\phi}, \sigma^2)$ where $\boldsymbol{\phi} \in \mathbb{R}^L$ is the vector of autoregressive parameters and L is the number of lags. For a given segment $\mathbf{y}_{j,s:t} = \{y_{j,s+1}, \dots, y_{j,t}\}$, the likelihood is then given by

$$f_j(\mathbf{y}_{j,s:t}|\boldsymbol{\phi}, \sigma^2) = \mathcal{N}_{t-s}(\mathbf{y}_{j,s:t}|\mathbf{H}_{j,st}\boldsymbol{\phi}, \sigma^2\mathbf{I}_{t-s}) \quad (5)$$

where $\mathcal{N}_{t-s}(\cdot|\boldsymbol{\mu}, \boldsymbol{\Sigma})$ denotes the density of the $t-s$ dimensional normal distribution, \mathbf{I}_{t-s} denotes the $(t-s) \times (t-s)$ identity matrix and

$$\mathbf{H}_{j,st} = \begin{bmatrix} y_{j,s} & y_{j,s-1} & \cdots & y_{j,s-L+1} \\ y_{j,s-1} & y_{j,s-2} & \cdots & y_{j,s-L} \\ \vdots & \vdots & \ddots & \vdots \\ y_{j,t-1} & y_{j,t-2} & \cdots & y_{j,t-L} \end{bmatrix} \quad (6)$$

is a $(t-s) \times L$ matrix with rows containing the lagged values for each observation in the segment. We place a conjugate normal-inverse-gamma prior over $\theta = (\boldsymbol{\phi}, \sigma^2)$:

$$f_j(\phi_l|\sigma^2) = \mathcal{N}(\phi_l|0, \delta_{j,l}\sigma^2) \text{ for } l = 1, \dots, L \quad (7)$$

$$f_j(\sigma^2) = \mathcal{IG}(\sigma^2|\alpha_j, \beta_j) \quad (8)$$

where $\mathcal{IG}(\sigma^2|\alpha, \beta)$ denotes the density of the inverse gamma distribution and $(\alpha_j, \beta_j, \delta_{j,1}, \dots, \delta_{j,L})$ are a set of hyperparameters for series j . Integrating over $(\boldsymbol{\phi}, \sigma^2)$ within a given segment, we obtain the marginal segment density:

$$f_j(\mathbf{y}_{j,s:t}) = (2\pi)^{-(t-s)/2} \left(\frac{|\mathbf{D}_{j,st}|}{|\mathbf{D}_j|} \right)^{1/2} \frac{\beta_j^{\alpha_j} \Gamma(\alpha_{j,st})}{\beta_{j,st}^{\alpha_{j,st}} \Gamma(\alpha_j)} \quad (9)$$

where $\Gamma(\cdot)$ denotes the gamma function, $\mathbf{D}_j = \text{diag}(\delta_{j,1}, \dots, \delta_{j,L})$, $\alpha_{j,st} = \alpha_j + (t-s)/2$, $\beta_{j,st} = \beta_j + \frac{1}{2}[\|\mathbf{Y}_{j,s:t}\|_2^2 - \mathbf{E}_{j,st}\mathbf{D}_{j,st}\mathbf{E}_{j,st}^T]$, $\mathbf{E}_{j,st} = \mathbf{Y}_{j,s:t}\mathbf{H}_{j,st}$ and $\mathbf{D}_{j,st} = (\mathbf{H}_{j,st}^T\mathbf{H}_{j,st} + \mathbf{D}_j^{-1})^{-1}$. This likelihood model was previously considered by Fearnhead and Liu (2007) in the univariate setting and may be used to model data with a constant mean but which exhibits change-points in the variability and/or autocorrelation structure.

In practice, it is essential to carefully select the hyperparameters $(\alpha_j, \beta_j, \delta_{j,1}, \dots, \delta_{j,L})$ for each series to minimise the error rate in the change-point locations. A fully Bayesian approach involves placing priors on these parameters and updating them during posterior sampling. However, fixing the parameters can yield substantial computational savings, as each marginal segment density must only be computed once and can be reused. In the examples presented in Section 4, we present sensible default values.

2.2 Change-Point Prior

The change-point locations in each series are determined by the multivariate hidden state process $\{\mathbf{X}_t\}_{t=1, \dots, T}$ where $\mathbf{X}_t = (X_{1,t}, \dots, X_{d,t})'$ is the vector containing the times of the most recent change-point before time t for each series. Since the first segment in each series starts at time $t = 1$, the process is initialised by

$$X_{j,1} \stackrel{a.s.}{=} 0 \quad \forall j = 1, \dots, d \quad (10)$$

and then for $t = 2, \dots, T$ we have $\mathbf{X}_t \in \{0, \dots, t-1\}^d$, with the event $X_{j,t} = t-1$ indicating a change-point occurred at time t in series j . Our prior over the hidden states assumes that the process $\{\mathbf{X}_t\}_{t=1, \dots, T}$ follows a Markov chain initialised by Equation (10) with time varying transition probabilities given by

$$\Pr(\mathbf{X}_t = \mathbf{x}_t | \mathbf{X}_{t-1} = \mathbf{x}_{t-1}) = \prod_{j=1}^d \Pr(X_{j,t} = x_{j,t} | \mathbf{X}_{t-1} = \mathbf{x}_{t-1}) \quad (11)$$

where

$$\Pr(X_{j,t} = x_{j,t} | \mathbf{X}_{t-1} = \mathbf{x}_{t-1}) = \begin{cases} p_{j,t}(\mathbf{x}_{t-1}), & \text{if } x_{j,t} = t-1 \\ 1 - p_{j,t}(\mathbf{x}_{t-1}), & \text{if } x_{j,t} = x_{j,t-1} \end{cases} \quad (12)$$

Conditional on $\mathbf{X}_{t-1} = \mathbf{x}_{t-1}$, the prior probability that a change-point occurs at time $t-1$ in series j is given by $p_{j,t}(\mathbf{x}_{t-1})$. The dependence in the change-point locations across the series is controlled by our choice of $p_{j,t}(\mathbf{x}_{t-1})$.

A natural starting point in specifying $p_{j,t}(\mathbf{x}_{t-1})$ is to consider independent univariate change-point priors for each series j . A popular choice is the Bernoulli process (see Yao, 1984; Barry and Hartigan, 1993; Fearnhead, 2006), which specifies

$$p_{j,t}(\mathbf{x}_{t-1}) = q_{0,j} \quad \text{for } j = 1, \dots, d \quad (13)$$

for $q_{0,j} \in (0, 1)$ which implies that the change-point probabilities in each series are constant for all t . This is equivalent to the change-point locations in each series j being generated by a renewal process with geometrically distributed inter-arrival times where $q_{0,j}$ is the distribution parameter. Similar to the approach of Hallgren et al. (2024), we use the Bernoulli process as a starting point such that, in the case of no dependence, our prior defaults to Equation (13).

Motivated by lead-lag relationships in change-points in different series, if a given series i leads series j , then $p_{j,t}(\mathbf{x}_{t-1})$ should depend on $x_{i,t-1}$. That is, the probability of a change-point occurring in series j should depend on the distance to the most recent change-point in series i . As noted earlier, we represent this dependence via a weighted directed graph. Let $\mathbf{A} \in \{0, 1\}^{d \times d}$ be an adjacency matrix, with elements $A_{i,j}$ controlling which pairs of series exhibit lead-lag relationships. Let $\mathbf{W}_0 \in \mathbb{R}_+^d$ be a vector of positive weights, and $\mathbf{W} \in \mathbb{R}_+^{d \times d}$ a matrix of positive weights with elements $W_{i,j}$ controlling the strength of the lead-lag relationships. Finally, let $g_{i,j} : \mathbb{Z}_+ \mapsto [0, 1]$ be a set of pre-specified functions, with the function $g_{i,j}$ controlling the delay effect of a change-point in series j following a change-point in series i .

Then our model for $p_{j,t}(\mathbf{x}_{t-1})$ with the latent weighted directed graph is given by:

$$p_{j,t}(\mathbf{x}_{t-1}) = Z_j^{-1} \left(W_{0,j} q_{0,j} + \sum_{i=1}^d A_{i,j} W_{i,j} g_{i,j}(t - x_{i,t-1} - 1) I(x_{i,t-1} > 0) \right) \quad (14)$$

where Z_j is a normalising constant given by

$$Z_j = W_{0,j} + \sum_{i=1}^d A_{i,j} W_{i,j} \quad (15)$$

and $I(x_{i,t-1} > 0)$ the indicator function preventing the model from treating $t = 0$ as an observed change-point. The normalised version of Equation (14) is given by:

$$p_{j,t}(\mathbf{x}_{t-1}) = W_{0,j}^* q_{0,j} + \sum_{i=1}^d W_{i,j}^* g_{i,j}(t - x_{i,t-1} - 1) I(x_{i,t-1} > 0) \quad (16)$$

where $W_{0,j}^* = W_{0,j}/Z_j$ and $W_{i,j}^* = A_{i,j}W_{i,j}/Z_j$ with $\sum_{i=0}^d W_{i,j}^* = 1$ are normalized weights. Equation (16) shows that the event of a change-point occurring at time t in series j is a mixture of $d + 1$ Bernoulli trials. This mixture consists of the independent Bernoulli prior and a contribution from the lead-lag relationship between the i th series and j th series, (i.e. those that are connected to j on the graph with $A_{i,j} = 1$). The contribution of a connected series i at a given time t depends on the distance $(t - x_{i,t-1} - 1)$ to the most recent change-point in that series.

From Equation (14) we can see that if $A_{i,j} = 0 \forall (i, j)$ or $d = 1$ then we recover the independent Bernoulli prior (13) applied to each series. However, if $d > 1$ and $A_{i,j} = 1$ for some (i, j) , then the probability of a change-point occurring in series j at a given time t depends on the distance to the most recent change-point in series i . Since, $W_{i,j}$ and $g_{i,j}$ are strictly positive, a recent change in i will cause an increase in the probability of a change occurring in j shortly after. The magnitude of this increase is controlled by $W_{i,j}$ and the delay effect by $g_{i,j}$. Finally, the background weights $W_{0,j}$ control the contribution from the independent Bernoulli process (with parameter $q_{0,j}$) for each series j .

The choice of function $g_{i,j}$ depends on our prior beliefs regarding the delay in change-points between two dependent series. If we expect short delays, then we may choose a function which decays as the distance to the most recent change-point increases. A natural choice here is to use the probability mass function (PMF) of the geometric distribution:

$$g_{i,j}(t) = q_{i,j}(1 - q_{i,j})^{t-1} \quad (17)$$

for some $q_{i,j} \in (0, 1)$. Under this choice, change-points in a lagging series are most likely to occur shortly after those in the corresponding leading series. The delay can be controlled through the geometric decay parameters $\mathbf{q} = (q_{i,j})$, with a larger $q_{i,j}$ inducing a faster decay and shorter delays.

We assume $g_{i,j}$ is given by the geometric PMFs in Equation (17) and so our prior on the hidden states, \mathbf{X}_t , is parametrised by $(\mathbf{W}_0, \mathbf{W}, \mathbf{A}, \mathbf{q}_0, \mathbf{q})$. For brevity, we will suppress conditioning on $(\mathbf{W}_0, \mathbf{W}, \mathbf{A}, \mathbf{q}_0, \mathbf{q})$, implicitly assuming that any probabilities involving the hidden state process \mathbf{X}_t depend on these parameters. In Section 2.3 we discuss how these parameters affect the properties of the hidden state process and hence the locations of the change-points.

2.3 Properties of the Prior

In this Section we assume that the hidden state hyperparameters $(\mathbf{W}_0, \mathbf{W}, \mathbf{A}, \mathbf{q}_0, \mathbf{q})$ are known and in Section 2.4 we discuss sensible hyperpriors for these. Recall that our prior on the hidden states is constructed such that when $\mathbf{A} = \mathbf{0}$, the change-points occur independently in each series according to a Bernoulli process with parameter $q_{0,j}$. When $\mathbf{A} \neq \mathbf{0}$, we have dependence between pairs of series (i, j) for which $A_{i,j} \neq 0$.

A first step to understanding this dependence is to simulate a realisation of \mathbf{X}_t and the corresponding probabilities $p_{j,t}$. Figure 1a displays a realisation of \mathbf{X}_t for $d = 3$. Here, \mathbf{A} corresponds to a chain graph such that the second series depends on the first series and the third depends on the second. The change-points in the first series occur independently according to a Bernoulli process with parameter $q_{1,0}$. However, when a change occurs in the first series, the change probabilities in the second series experience an impulse response. This impulse response decays over time, due to the geometric function in Equation (17). This increases the likelihood that changes in the second series follow those in the first series shortly after, producing a lead-lag relationship in the change locations. The same effect is observed between series two and three, due to the directed edge between them.

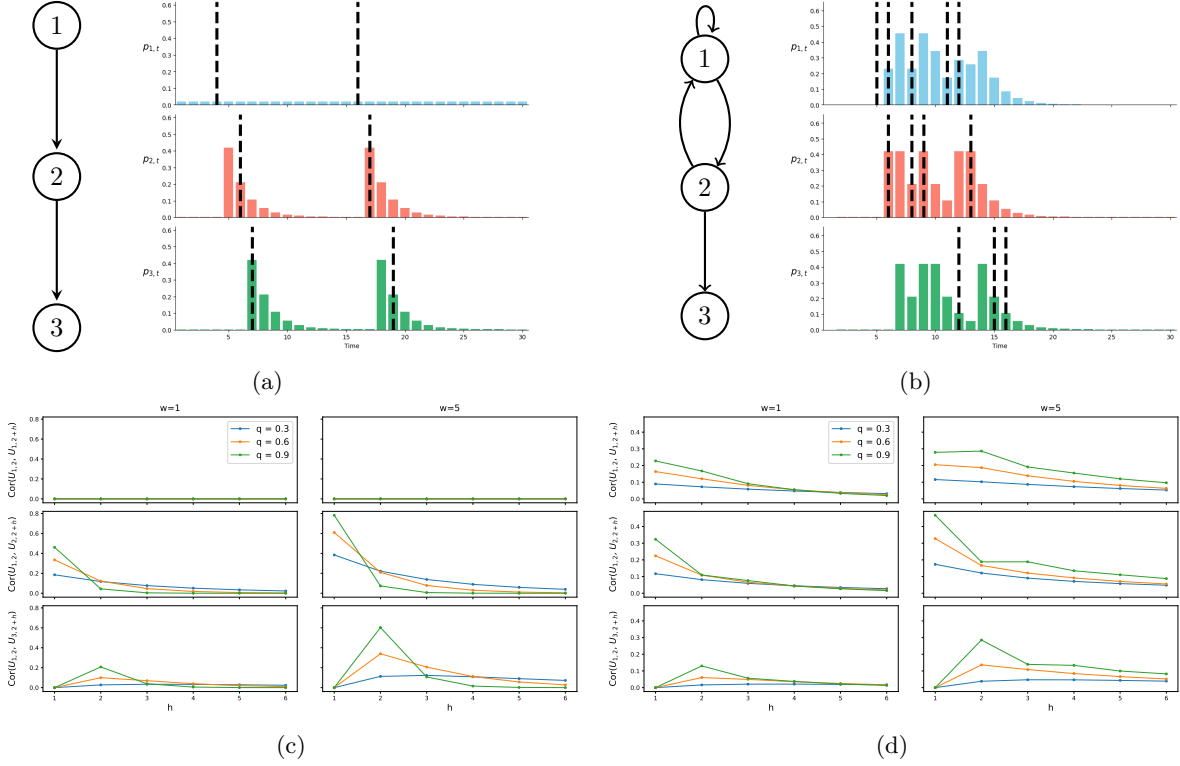


Figure 1: (a)–(b) Simulated change-point processes \mathbf{X}_t with $d = 3$, using a chain graph structure for \mathbf{A} in (a) and a cyclic graph in (b). Bars represent the probabilities $p_{j,t}$, and dashed lines indicate the change-point locations. Parameters are the same for both cases: $\mathbf{q}_0 = \frac{1}{50} \mathbf{1}_3$, $\mathbf{W}_0 = \mathbf{1}_3$, $\mathbf{q} = \frac{1}{2} \mathbf{1}_{3 \times 3}$, and $\mathbf{W} = \mathbf{1}_{3 \times 3}$; (c)–(d) Cross-correlation function $Cor(U_{1,2}, U_{j,2+h})$ for $j = 1$ (top), $j = 2$ (middle), and $j = 3$ (bottom), with \mathbf{A} as a chain graph in (c) and a cyclic graph in (d). Each column corresponds to a different edge weight w , and within each plot, curves show the effect of varying decay parameter q .

However, graphs that contain cycles can exhibit problematic dynamics, where bursts of consecutive change-points become likely due to excessive positive feedback. This effect is illustrated in Figure 1b, where a change-point in the first series triggers an impulse response not only in the change-point probabilities of the second series two but also in its own. A subsequent change in the second series then feeds back into the first one, creating mutually reinforcing impulses. These feedback loops result in clusters of change-points occurring in quick succession. Such behaviour is typically undesirable because it leads to overfitting, where the model interprets random noise as meaningful structure, resulting in spurious change-point detections, reduced interpretability, and poor generalization to new data. Therefore, we should place little or no prior mass on cyclic graph structures, as further discussed in Section 2.4.

While the adjacency matrix \mathbf{A} controls which pairs of series exhibit dependence, the degree of dependence is controlled by $(W_{i,j}, q_{i,j})$. To quantify this dependence, we calculate the *a priori* correlation in the change-point locations at different lags for two given series. To do so we introduce a set of indicator variables $U_{j,t}$ defined as

$$U_{j,t} = \begin{cases} 1, & \text{if } X_{j,t} = t - 1 \\ 0, & \text{if } X_{j,t} = x_{j,t-1} \end{cases} \quad (18)$$

i.e. $U_{j,t} = 1$ indicates the presence of a change-point in series j at time $t - 1$. Then, for any two series (i, j) we compute $Cor(U_{i,t}, U_{j,t+h})$ for varying lags h . These correlations can be computed using a recursive calculation over the joint distribution of $\{\mathbf{X}_s\}_{s=1, \dots, t+h}$. In particular, for a given function

$k(\cdot, \cdot)$, we can compute $\mathbb{E}(k(\mathbf{X}_s, \mathbf{X}_t))$, for $t \geq s$, as

$$\begin{aligned} \mathbb{E}(k(\mathbf{X}_s, \mathbf{X}_t)) &= \sum_{\mathbf{x}_1 \in \mathcal{X}_1} \cdots \sum_{\mathbf{x}_t \in \mathcal{X}_t} Pr(\mathbf{X}_1 = \mathbf{x}_1, \dots, \mathbf{X}_t = \mathbf{x}_t) k(\mathbf{x}_s, \mathbf{x}_t) \\ &= \sum_{\mathbf{x}_2 \in \mathcal{X}_2} Pr(\mathbf{X}_2 = \mathbf{x}_2 | \mathbf{X}_1 = \mathbf{x}_1) \cdots \sum_{\mathbf{x}_t \in \mathcal{X}_t} Pr(\mathbf{X}_t = \mathbf{x}_t | \mathbf{X}_{t-1} = \mathbf{x}_{t-1}) k(\mathbf{x}_s, \mathbf{x}_t) \end{aligned} \quad (19)$$

where $\mathcal{X}_t = \{0, 1, \dots, t-1\}^d$ is the support set of \mathbf{X}_t . The calculation in Equation (19) can easily be performed on a computer in low dimensions ($d < 5$) and allows us to compute $\mathbb{E}(U_{i,t})$, $\mathbb{E}(U_{j,t+h})$, $\mathbb{E}(U_{i,t}U_{j,t+h})$ and hence $\text{Cor}(U_{i,t}, U_{j,t+h})$ for varying h .

Figure 1c displays the correlations across the change-point locations for varying edge weights and decay parameters where \mathbf{A} is a chain graph described in Figure 1a. The rows correspond to the correlations between a change-point in the first series at time 2 and a change-point in the j th series at times $2+h$ for $j = 1, 2, 3$ and $h = 1, \dots, 6$. Under this choice of \mathbf{A} , we see that the change-points in the first series exhibit no autocorrelation, since they occur independently. In contrast, the middle and bottom rows show non-zero correlations for the second and third series respectively, highlighting the directed dependencies from the first series to the second series and from the second series to the third. Note that the bottom row exhibits a one-step delay in correlation, reflecting the sequential propagation of a change-points from series to series. We can also see that increasing the edge weights increases the degree of correlation between pairs of series while increasing the geometric parameters, $q_{i,j}$, increases the rate of decay in the correlations. This analysis may be used to guide the specification of hyperpriors over the edge weights and geometric parameters.

Figure 1d displays the correlations induced by the cyclic graph displayed in Figure 1b. Focusing on the non-zero correlations in the first row, it is clear that the change-point indicators for the first series exhibit autocorrelation. This is expected and it reflects the positive feedback loops creating bursts of consecutive change-points which, as discussed previously, generate undesirable behaviour.

2.4 Hyperpriors

Motivated by our analysis of the hidden state process in Section 2.3, we now specify priors over the processes parameters $(\mathbf{W}_0, \mathbf{W}, \mathbf{A}, \mathbf{q}_0, \mathbf{q})$. A standard prior used to model random graphs is the Erdős-Rényi (ER) model (Erdős and Rényi, 1959), which specifies $A_{i,j} \stackrel{\text{iid}}{\sim} \text{Bern}(\rho)$ for $\rho \in (0, 1)$. This prior assigns equal probability, ρ , to each edge being present in the graph. Our analysis in Section 2.3 suggests that the presence of cycles in the graph may result in undesirable behaviour in the change-point locations and so we would like our prior to assign little or no mass on such graphs.

Constructing a prior which assigns non-zero mass only to directed acyclic graphs is difficult due to the space being combinatorially complex and highly constrained by acyclicity. We instead base our prior on a modification of the ER model which does not allow self edges or parallel edges. Specifically, we let $\rho \in (0, 1)$, and define our prior on \mathbf{A} as

$$Pr(\mathbf{A} = \mathbf{a} | \rho) = \prod_{j=1}^d Pr(A_{j,j} = a_{j,j}) \prod_{j=1}^d \prod_{i=j+1}^d Pr(A_{i,j} = a_{i,j}, A_{j,i} = a_{j,i} | \rho) \quad (20)$$

where $Pr(A_{j,j} = 0) = 1$ and

$$Pr(A_{i,j} = a_{i,j}, A_{j,i} = a_{j,i} | \rho) = \begin{cases} \rho/2, & \text{if } a_{i,j} = 0, a_{j,i} = 1 \\ \rho/2, & \text{if } a_{i,j} = 1, a_{j,i} = 0 \\ 1 - \rho, & \text{if } a_{i,j} = 0, a_{j,i} = 0 \\ 0, & \text{if } a_{i,j} = 1, a_{j,i} = 1 \end{cases} \quad (21)$$

In other words, for each pair of distinct vertices (i, j) with $i \neq j$, a directed edge is included with probability ρ , and omitted with probability $1 - \rho$. Under this choice, the expected number of edges is $\rho d(d-1)/2$, allowing us to control the sparsity of the graph through our prior on ρ . To encourage sparse graphs, we place a uniform prior with parameters $(0, 0.2)$ on ρ .

We choose independent Gamma priors for the background and edge weights, $(\mathbf{W}_0, \mathbf{W})$, i.e.

$$W_{0,j} \sim Ga(1, 1) \quad \text{for } j = 1, \dots, d \quad (22)$$

$$W_{i,j} \sim Ga(1, 1) \quad \text{for } i = 1, \dots, d; j = 1, \dots, d \quad (23)$$

where $Ga(a, b)$ denotes the Gamma distribution with shape a and rate b . We find that this choice works well when modelling the dependence between pairs of lead-lag series. Under this choice, we are centering the weights around one, producing correlations in the lagged change-point locations less than 0.5, see Figure 1c. This choice has the added property that the induced prior on the vector of normalised weights for series j is

$$(W_{0,j}^*, W_{1,j}^*, \dots, W_{d,j}^*) | \mathbf{A} \sim Dir(1, A_{1,j}, \dots, A_{d,j})$$

where $Dir(\alpha_1, \dots, \alpha_K)$ is the K dimensional Dirichlet distribution, with $\alpha_k = 0$ indicating that the k^{th} element in the sampled vector is zero almost surely.

Recall that the parameters $q_{i,j} \in (0, 1)$ control how quickly the correlation between a change-point in series i and a subsequent change-point in series j decays over time. Larger values result in a faster decay rate, indicating a change-point in the j th series is most likely to immediately follow a change-point in the i th series. Smaller values of $q_{i,j}$ allow for a longer delay. We choose the standard uniform prior:

$$q_{i,j} \sim \text{Uniform}(0, 1) \quad \text{for } i = 1, \dots, d; j = 1, \dots, d \quad (24)$$

to reflect the absence of any prior information on the decay rate. For this reason we also choose the standard uniform prior for the background rates $q_{j,0}$ which control the overall rate at which change-points occur in each series.

3 Posterior Inference

We now describe how to perform posterior inference for the NetCP model introduced in Section 2. Our MCMC sampler extends the work of Fearnhead (2006) and Whiteley et al. (2011) to the multivariate setting. We show how the hidden states for each series can be efficiently sampled in blocks using the forward-backward recursions of Fearnhead (2006). For long time series, we demonstrate how particle MCMC methods (Andrieu et al., 2010; Whiteley et al., 2011) can be used to control computational cost while preserving a high level of sampling efficiency.

The full joint posterior density is given by

$$\pi(\mathbf{x}, \mathbf{W}_0, \mathbf{W}, \mathbf{A}, \mathbf{q}_0, \mathbf{q}, \rho | \mathbf{y}) \propto f(\mathbf{y} | \mathbf{x}) Pr(\mathbf{X} = \mathbf{x} | \mathbf{W}_0, \mathbf{W}, \mathbf{A}, \mathbf{q}_0, \mathbf{q}) f(\mathbf{W}_0) f(\mathbf{W}) f(\mathbf{A} | \rho) f(\rho) f(\mathbf{q}_0) f(\mathbf{q}) \quad (25)$$

The main difficulty arises when sampling the hidden states, \mathbf{X} . One approach is to sample each $X_{j,t}$ one at a time from its full posterior conditional (see Barry and Hartigan, 1993; Quinlan et al., 2024). Since each $X_{j,t}$ is either $t - 1$ (a change-point) or $X_{j,t-1}$ (no change-point), this can be performed with simple Bernoulli samples. While easy to implement, strong dependencies between the $X_{j,t}$ mean that this method tends to mix poorly (see Fan and Mackey, 2017). Another popular approach is to use reversible jump MCMC (Green, 1995), but again this is sub-optimal since designing efficient proposal moves is non trivial.

We construct an efficient sampling scheme by sampling the hidden states in each series as a block. This may be done using the method of Fearnhead (2006), which employs a set of forward-backward recursions. However, these recursions have a computational cost of $\mathcal{O}(T^2)$ per series, making them impractical within an MCMC framework. To balance sampling efficiency with computational cost, we instead use the particle approximation of Whiteley et al. (2011), maintaining the correct stationary distribution via conditional particle filtering within a particle Gibbs framework (Andrieu et al., 2010). A single iteration of our sampling scheme involves the following steps:

1. For $j = 1, \dots, d$, sample $\mathbf{x}_{j,0:T}$ from $\pi(\mathbf{x}_{j,0:T} | \mathbf{y}, \mathbf{x}_{(-j),0:T}, \dots)$ via a particle Gibbs step.
2. Sample $(\mathbf{W}_0, \mathbf{W}, \mathbf{A}, \mathbf{q}_0, \mathbf{q}, \rho)$ from their full posterior conditionals.

We sample the static parameters in step 2 using standard Gibbs/Metropolis steps, the details of which can be found in Appendix A.

For the remainder of this section we discuss our blocked sampling scheme for the hidden states $\mathbf{x}_{j,0:T}$ for $j = 1, \dots, d$. Step 1 requires us to sample from the joint PMF of the hidden states in a given series j that is,

$$\pi(\mathbf{x}_{j,0:T} | \mathbf{y}, \mathbf{x}_{(-j),0:T}, \dots) \propto Pr(\mathbf{X}_{j,0:T} = \mathbf{x}_{j,0:T} | \mathbf{X}_{(-j),0:T} = \mathbf{x}_{(-j),0:T}) f_j(\mathbf{y}_{j,0:T} | \mathbf{x}_{j,0:T}) \quad (26)$$

Observe that due to the Markov properties of \mathbf{X}_t , the term $Pr(\mathbf{X}_{j,0:T} = \mathbf{x}_{j,0:T} | \mathbf{X}_{(-j),0:T} = \mathbf{x}_{(-j),0:T})$ can be factorised as

$$Pr(\mathbf{X}_{j,0:T} = \mathbf{x}_{j,0:T} | \mathbf{X}_{(-j),0:T} = \mathbf{x}_{(-j),0:T}) \propto Pr(X_{j,1} = x_{j,1}) \prod_{t=2}^T P_t^{(j)}(x_{j,t} | x_{j,t-1}, \mathbf{x}_{(-j),0:T}) \quad (27)$$

where the term $P_t^{(j)}(x_{j,t} | x_{j,t-1}, \mathbf{x}_{(-j),0:T})$ defines a transition PMF for $(X_{j,t} | X_{j,t-1}, \mathbf{X}_{(-j),0:T})$ and is defined up to proportionality as

$$P_t^{(j)}(x_{j,t} | x_{j,t-1}, \mathbf{x}_{(-j),0:T}) \propto \begin{cases} Pr(X_{j,t} = x_{j,t} | \mathbf{X}_{t-1} = \mathbf{x}_{t-1}^{[j=x_{j,t-1}]}) \prod_{i \neq j}^d Pr(X_{i,t+1} = x_{i,t+1} | \mathbf{X}_t = \mathbf{x}_t^{[j=x_{j,t}]}), & \text{for } 2 \leq t < T \\ Pr(X_{j,t} = x_{j,t} | \mathbf{X}_{t-1} = \mathbf{x}_{t-1}^{[j=x_{j,t-1}]}), & \text{for } t = T \end{cases} \quad (28)$$

where $\mathbf{x}^{[j=s]} = (x_1, \dots, x_{j-1}, s, x_{j+1}, \dots, x_d)^T$, denotes the vector \mathbf{x} with the value s imputed at the j^{th} index. The hidden state at time t can take two values ($t-1$ or $x_{j,t-1}$), and so the normalizing constant of $P_t^{(j)}(x_{j,t} | x_{j,t-1}, \mathbf{x}_{(-j),0:T})$ can be easily found. Therefore, conditional on the hidden states in all other series, the hidden states in series j follow Markov a chain, with transitions given by (28). Recall that the likelihood for series j can be factorised as

$$f_j(\mathbf{y}_{j,0:T} | \mathbf{x}_{j,0:T}) = \prod_{t=1}^T f_j(y_{j,t} | x_{j,t}, \mathbf{y}_{j,0:t-1}) \quad (29)$$

where $f_j(y_{j,t} | x_{j,t}, \mathbf{y}_{j,0:t-1})$ is given by (4). The full posterior conditional (26) can therefore be written as

$$\pi(\mathbf{x}_{j,0:T} | \mathbf{y}, \mathbf{x}_{(-j),0:T}, \dots) \propto f_j(y_{j,1}) \prod_{t=2}^T P_t^{(j)}(x_{j,t} | x_{j,t-1}, \mathbf{x}_{(-j),0:T}) f_j(y_{j,t} | x_{j,t}, \mathbf{y}_{j,0:t-1}) \quad (30)$$

where $x_{j,1} = 0$ as per Equation (10).

The manner in which Equation (30) factorises allows us to use the forward-backward recursions of Fearnhead (2006) to perform direct sampling. However, due to the $\mathcal{O}(T^2)$ computational time needed for the exact recursions, we instead use a the of the method of Whiteley et al. (2011) to replace the exact filtering distributions at time t with an approximation. This approximation consists of N weighted particles and reduces the computational cost to $\mathcal{O}(NT)$. A key component in the method of Whiteley et al. (2011) is the particle filter of Fearnhead and Liu (2007). It differs from standard particle methods in two ways. First, since the state space is discrete, a deterministic search of the proposal space is used instead of a random proposal, a strategy which greatly reduces Monte Carlo error. Second, instead of using multinomial resampling, it employs Stratified Optimal Resampling (SOR), which is shown to be optimal over all existing unbiased resampling methods in terms of the maximum Kolmogorov–Smirnov distance. This approach ensures that no duplicate particles are stored at each iteration, since there is no advantage in storing multiple copies in a discrete space (see Fearnhead and Liu, 2007).

Algorithm 1 describes the resulting particle Gibbs update for $\mathbf{x}_{j,0:T}$. In the following, we denote the set of particles at time t by $\mathcal{S}_t \subseteq \{0, \dots, t-1\}$ and their associated weights by $\mathcal{W}_t = \{w_t(s_t)\}_{s_t \in \mathcal{S}_t}$. Thus, at time t , the particle $s \in \mathcal{S}_t$ has weight $w_t(s)$.

Algorithm 1 Particle Gibbs update of $\mathbf{x}_{j,0:T}$

Require: \mathbf{x}^* (current hidden state matrix), N (number of particles).

- 1: At time $t = 1$, set $\mathcal{S}_1 = \{0\}$ and $\mathcal{W}_1 = \{1\}$.
 - 2: **for** $t = 2, \dots, T$ **do**
 - 3: Set $\mathcal{S}_t = \mathcal{S}_{t-1} \cup \{t-1\}$.
 - 4: For each $s_{t-1} \in \mathcal{S}_{t-1}$ set $w_t(s_{t-1}) \propto w_{t-1}(s_{t-1}) P_t^{(j)}(s_{t-1} | s_{t-1}, \mathbf{x}_{(-j),0:T}^*) f_j(y_{j,t} | s_{t-1}, \mathbf{y}_{j,0:t-1})$
 - 5: Set $w_t(t-1) = f_j(y_{j,t}) \sum_{s_{t-1} \in \mathcal{S}_{t-1}} w_{t-1}(s_{t-1}) P_t^{(j)}(t-1 | s_{t-1}, \mathbf{x}_{(-j),0:T}^*)$
 - 6: Normalise the weights \mathcal{W}_t such that $\sum_{s_t \in \mathcal{S}_t} w_t(s_t) = 1$.
 - 7: If $|\mathcal{S}_t| > N$, resample $(\mathcal{S}_t, \mathcal{W}_t)$ using the Conditional SOR algorithm (conditional on $\mathbf{x}_{j,t}^*$).
 - 8: **end for**
 - 9: Given $\{(\mathcal{S}_t, \mathcal{W}_t)\}_{t=1, \dots, T}$ generate a new sample $\mathbf{x}_{j,0:T}$ using the backward sampling algorithm.
-

Algorithm 1 requires additional algorithms to perform the resampling in step 7 and backward sampling in step 9. These algorithms are the same as those given in Whiteley et al. (2011) and can be found in the Appendix A.

Note that if the number of particles N is set to T , then we never perform resampling in step 7 and Algorithm 1 is equivalent to the exact filtering recursions of Fearnhead (2006). However, when $N < T$, the sampler maintains the correct stationary distribution due to conditioning on the previous sample (Andrieu et al., 2010). In our simulated and real datasets we find that relatively few particles ($N \approx 200$) are required to obtain mixing similar to that of the direct sampling method where $N = T$. An analysis of the efficiency of our particle Gibbs scheme compared to the single site Gibbs sampler can be found in Appendix B.

A key assumption in Algorithm 1 is that the segment specific parameters may be marginalised out of the model, producing a Rao-Blackwellized filtering scheme. This results in highly efficient Monte Carlo estimates although restricts us to specifying conjugate segment likelihood models. In cases where non-conjugate models are used, the particle filter of Fearnhead and Liu (2007) may be replaced with that of Chopin (2006). Here, the segment specific parameters may be left in the model and included in the filtering steps, albeit at an increased computational cost and a reduction in Monte Carlo efficiency.

Finally, we point out that it is trivial to modify the above particle Gibbs step to sample from the posterior of multivariate Markov chains other than the change-point model presented here. This is possible as long as the transition PMF is in the form given in (11) and the likelihood factorises according to (2). The updating in steps 3-5 of Algorithm 1 can be replaced with the more general particle filter of Fearnhead and Clifford (2003), allowing for Markov models which could re-enter previous states.

4 Illustrations

In this section we evaluate the performance of NetCP in modelling change-points and inferring the underlying graph structure using both simulated and real data examples.

4.1 Simulation Study

We first perform a simulation study to test

- (i) NetCP’s ability to perform edge link analysis on the true graph generating the change-points.
- (ii) NetCP’s fit, in terms of log model evidence, against several competing methods.

We consider five scenarios for the change-point generating process and two possible segment likelihood models, resulting in 10 distinct data generating scenarios. Our change-point scenarios are designed to test situations in which change-points in different series (a) exhibit lead-lag relationships, (b) occur simultaneously across all, or subsets of the series and (c) are independent. Below we provide a description of each scenario **S1** - **S5**.

- S1** Simulate from the NetCP model with parameters $\mathbf{W}_0 = \mathbf{1}_4$ and $\mathbf{q}_0 = \frac{1}{40}\mathbf{1}_4$. We use an adjacency matrix corresponding to a chain graph with $A_{1,2} = A_{2,3} = A_{3,4} = 1$ and all other $A_{i,j} = 0$. The edge weights are set to $W_{1,2} = W_{2,3} = W_{3,4} = 5$ and the edge decay parameters to $q_{1,2} = q_{2,3} = q_{3,4} = 0.6$. The correlations induced by this choice can be seen in Figure 1c.
- S2** Simulate from the NetCP model with the same parameters as **S1** but instead setting $A_{2,3} = 0$, resulting in two sub-graphs.
- S3** Simulate the change-points simultaneously in all series. The change-point locations follow a Bernoulli process with parameter $1/40$.
- S4** Simulate the change-points simultaneously in series 1 & 2 according to a Bernoulli process with parameter $1/40$. The change-points in series 3 & 4 are also generated simultaneously with an independent and identical Bernoulli process.
- S5** Change-points in each series are generated according to an independent Bernoulli process with parameter $1/40$.

For each change-point scenario (**S1** - **S5**), we generate data for two likelihood models. The first is the AR model presented in Equation (5). Under this scenario, the data in each segment of each series follows an AR(1) process, and the segment parameters (ϕ_1, σ^2) alternate between four possible states $\{(-0.8, 0.3^2), (0.8, 1^2), (-0.8, 2^2), (0.8, 3^2)\}$ for all series.

Many existing change-point models focus on detecting changes in means (Truong et al., 2020) and our second likelihood scenario is designed for this purpose. Under this scenario, the observations in each series are independent Gaussian with fixed variance σ_j^2 and piecewise constant means which are sampled independently from a $\mathcal{N}(0, \gamma_j^2)$ distribution. This likelihood model is conjugate and the corresponding marginal segment density can be found in Appendix C. For this scenario’s simulated data we set $\sigma_j^2 = 0.5$ and $\gamma_j^2 = 3$ for all series j . For each scenario and likelihood model, we generate 50 datasets, each with $d = 4$ time series and $T = 500$ time points.

To evaluate NetCP’s ability to perform edge link analysis in test (i) we need to assess the model’s output for **S1**, **S2** and **S5** (where **S5** corresponds to NetCP with an empty graph). Our aim is to check NetCP’s ability to correctly predict which edges (i, j) are in the graph. For each simulated dataset we calculate the Area Under the Receiver Operating Characteristic Curve (AUC) by thresholding the posterior edge inclusion probabilities $Pr(A_{i,j} = 1 | \mathbf{y})$. The AUC is then averaged over the 50 datasets for each change-point scenario and likelihood model.

When fitting the NetCP model on the AR process likelihood we set the hyperparameters $\alpha_j = \beta_j = \delta_{j,1} = 1$ for all series j . For the Gaussian likelihood model we set the hyperparameters to the true values $\sigma_j^2 = 0.5$ and $\gamma_j^2 = 3$ for all series j . We then estimate the NetCP model using the particle Gibbs scheme with 150 particles and 5000 iterations, discarding the first 500 as burn-in.

	S1	S2	S5
Gaussian Mean	0.994 (0.919, 1.0)	0.998 (0.998, 1.0)	1.0 (1.0, 1.0)
AR Process	0.987 (0.87, 1.0)	0.989 (0.899, 1.0)	1.0 (1.0, 1.0)

Table 1: Average AUC and 5% quantiles for edge link analysis under the NetCP model for change-point scenarios **S1**, **S2** and **S5**.

Table 1 displays the AUC for the link analysis test. From this we can see that on a sample of $T = 500$ time points, the model is able to nearly perfectly recover the true 4×4 adjacency matrix from scenarios **S1**, **S2** and **S5**.

For test (ii) we compare NetCP’s network prior to three competing change-point priors. The first is the special case of NetCP obtained by setting $\mathbf{A} = \mathbf{0}$, which is equivalent to the Bernoulli prior of Yao (1984) being applied to each series independently. We refer to this model as the “Yao” model. We also consider the two priors proposed by Quinlan et al. (2024). The first is the Non-Global Correlated Change-Point PPM, which we refer to as “NG-CCP”. This prior is constructed by replacing the transition probabilities in (12) with

$$p_{j,t}(\mathbf{x}_{t-1}) = p_{j,t}^*, \quad \text{for } j = 1, \dots, d \quad (31)$$

$$(\text{logit}(p_{1,t}^*), \dots, \text{logit}(p_{d,t}^*)) \sim t_d(\nu, \mu, \Sigma) \quad (32)$$

where t_d denotes the d -dimensional t distribution. We also consider the “Global” prior of Quinlan et al. (2024), which we refer to as “G-CCP”, obtained by setting

$$p_{j,t}(\mathbf{x}_{t-1}) = p_j^*, \quad \text{for } j = 1, \dots, d \quad (33)$$

$$(\text{logit}(p_1^*), \dots, \text{logit}(p_d^*)) \sim t_d(\nu, \mu, \Sigma) \quad (34)$$

These priors encourage simultaneous change-points across series by allowing the change-point probabilities for a fixed time to be correlated through choice of (ν, μ, Σ) . Quinlan et al. (2024) do not provide priors for these parameters, however, they do provide a method to compute sensible default values. Both the G-CCP and NG-CCP models can be estimated using the particle Gibbs scheme described in Section 3 and the latent transition probabilities $p_{j,t}^*$ and p_j^* sampled using the Metropolis steps given in Quinlan et al. (2024).

In order to compare model performance, we use the MCMC output to estimate the log Bayes factor, relative to our NetCP model, for each competing model as

$$\log \text{BF}_M = \log f_M(\mathbf{y}) - \log f_{\text{NetCP}}(\mathbf{y})$$

where $\log f_M(\mathbf{y})$ is the log model evidence for model M . Positive values of $\log \text{BF}_M$ support model M over NetCP. Values in excess of five suggest strong support. Similarly negative values suggest support for NetCP. We compute $\log f_M(\mathbf{y})$ as follows,

$$\log f_M(\mathbf{y}) = \sum_{t=1}^T \log f_M(\mathbf{y}_t | \mathbf{y}_{0:t-1})$$

The posterior predictive likelihoods $f_M(\mathbf{y}_t | \mathbf{y}_{0:t-1})$ can be approximated by running the Gibbs sampler using the data up to time $t - 1$; at each iteration, the hidden state x_t is sampled, and the predictive likelihood is estimated by averaging the likelihood of observation \mathbf{y}_t over these sampled hidden states. To fit each model, we produce 5000 posterior samples using 150 particles and 500 burn-in. To achieve this we use the King’s College London (KCL) CREATE computing cluster.

	S1	S2	S3	S4	S5
NetCP	0 (0, 0)	0 (0, 0)	0 (0, 0)	0 (0, 0)	0 (0, 0)
Yao	-29.0 (-52.9, -6.2)	-17.2 (-30.3, -3.5)	-38.5 (-52.8, -17.9)	2.6 (-2.5, 7.6)	6.2 (4.6, 7.6)
G-CCP	-26.9 (-53.0, -2.9)	-15.1 (-28.4, 0.8)	-37.1 (-53.3, -14.7)	4.2 (-2.4, 11.5)	7.5 (4.7, 10.0)
NG-CCP	-41.8 (-85.6, -3.92)	-34.1 (-61.4, -8.8)	2.8 (-14.1, 21.2)	1.4 (-11.9, 15.0)	-15.8 (-33.3, -3.9)

Table 2: Average log Bayes Factors, $\log \text{BF}_M$, and 5% quantiles under each scenario for Gaussian mean likelihood. Highest average Bayes Factor for each scenario is marked in bold.

Table 2 displays the averaged log Bayes factors, relative to NetCP for each model under the normal means likelihood scenario. In **S1** and **S2**, which involve lead-lag relationships in change-points, NetCP clearly outperforms all other methods, with substantial negative log Bayes factors observed for competing models. In **S3**, where change-points occur simultaneously across series, NG-CCP achieves the highest score relative to NetCP, though the interval overlaps zero, suggesting comparable performance. In **S4**, G-CCP performs best, though differences between methods are again modest. For **S5**, which contains independent change-points across series, G-CCP yields the highest average Bayes factor, but Yao performs similarly, as indicated by their overlapping intervals. Overall, these results suggest that NetCP excels in structured, temporally misaligned settings, while G-CCP and Yao are more competitive in scenarios with simultaneous or independent change-points.

	S1	S2	S3	S4	S5
NetCP	0 (0, 0)	0 (0, 0)	0 (0, 0)	0 (0, 0)	0 (0, 0)
Yao	-17.8 (-32.3, -1.4)	-9.1 (-22.6, 0.8)	-55.3 (-74.2, -39.3)	-21.0 (-27.9, -14.7)	7.3 (5.4, 9.5)
G-CCP	-16.2 (-32.0, 1.2)	-8.2 (-21.1, 1.8)	-54.6 (-75.2, -36.8)	-20.1 (-27.4, -12.1)	8.1 (5.3, 11.0)
NG-CCP	-20.8 (-45.1, 2.3)	-21.7 (-39.3, -5.6)	-19.0 (-34.9, -2.8)	-25.2 (-41.6, -7.6)	-12.8 (-29.7, 1.4)

Table 3: Average log Bayes Factors, $\log \text{BF}_M$, and 5% quantiles under each scenario for AR process likelihood. Highest average Bayes Factor for each scenario is marked in bold.

Table 3 displays the same information as Table 2 but for the AR process likelihood scenario. Here NetCP performs strongly in **S1 - S4**, achieving the highest estimated log Bayes factors relative to all other methods. In **S1** and **S2**, which involve lead-lag relationships between change-points, alternative methods show moderately negative Bayes factors, with some intervals overlapping zero, suggesting marginally weaker but not clearly inferior performance. In **S3** and **S4**, which simulate simultaneous change-points, all competing methods perform substantially worse than NetCP, with large negative Bayes factors and tight intervals below zero. For **S5**, where change-points are independent across series, G-CCP achieves the highest Bayes factor, slightly outperforming Yao, although both perform better than NetCP in this setting. These results further support the advantage of NetCP in structured or temporally dependent change-point settings, while G-CCP and Yao remain competitive in less structured scenarios.

4.2 Seismology Data

For our first real example, we apply our model to the detection of microearthquakes using data from a network of seismic sensors. Specifically, we use recordings from the High Resolution Seismic Network

(HSRN), maintained by the UC Berkeley Seismology Laboratory (NCEC, 2014). This network comprises geophone sensors positioned around the town of Parkfield, California, and is designed to monitor seismic activity along the San Andreas fault. Similar data was previously analysed by Xie et al. (2019) who took a frequentist approach, focussing on estimating the relative delay between change-points in different series. For our analysis, we consider data from seven sensors over a 100 second period beginning at 22:32:10 on 28/09/2004. Each sensor samples at 20 Hz, yielding $T = 2000$ observations per series.

According to the Northern California Earthquake Catalogue¹ (NCEC), four microearthquakes (events with magnitude < 2.0) were recorded in Parkfield during this time. Prior to our analysis, we apply a 2-16 Hz Butterworth bandpass filter to each series, as is standard procedure in the seismology literature (Caudron et al., 2018). We then normalise each series to have zero mean and unit variance. For the likelihood model within each segment we use the AR model described in Equation (9), setting the lag to $L = 1$ and use hyperparameters $\alpha_j = \beta_j = \delta_{j,1} = 1$ for all series $j = 1, \dots, 7$. We then ran two MCMC chains in parallel for 20,000 iterations using the particle Gibbs scheme with 200 particles, discarding the first 2000 iterations of each chain as burn-in.

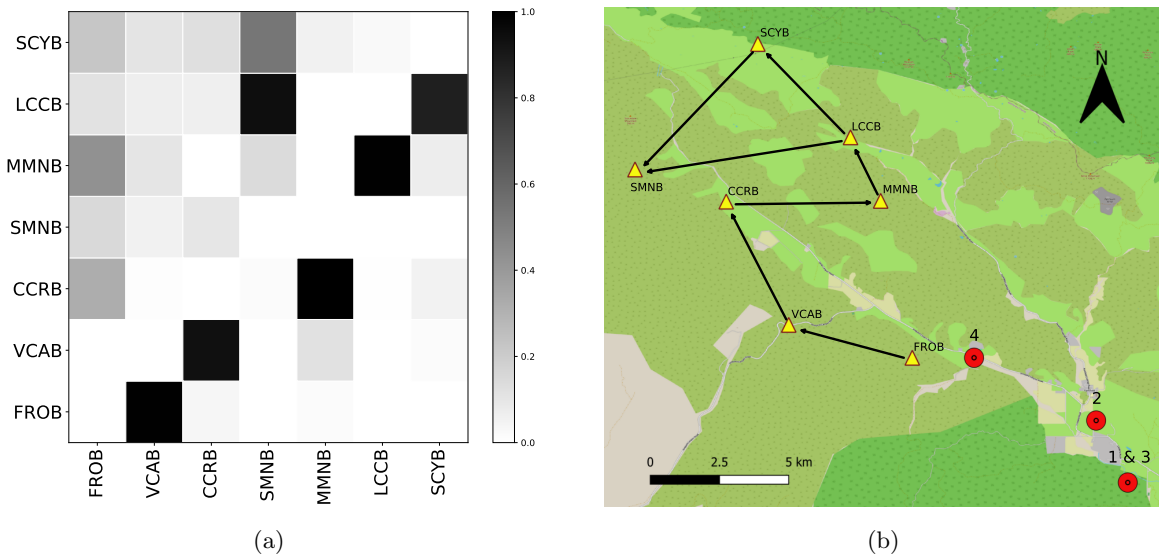


Figure 2: Network analysis of seismic sensor data: (a) Heatmap displaying estimated inclusion probabilities $Pr(A_{i,j} = 1|\mathbf{y})$. (b) Locations of the seven seismic sensors (yellow triangles) and the epicentres of the microearthquakes (red circles) labelled according to their order of occurrence. Arrows correspond to edges obtained after thresholding $Pr(A_{i,j} = 1|\mathbf{y})$ at 50%.

Figure 2 displays the posterior edge inclusion probabilities and sensor/microearthquake locations. We perform link edge analysis by thresholding $Pr(A_{i,j} = 1|\mathbf{y})$ at 50%. The resulting edges displayed in Figure 2b suggest that sensors nearer to Parkfield tend to lead the ones which are further away.

Figure 3 displays the processed data and posterior change-point probabilities for each station. According to the NCEC, the first microearthquake occurs at 22:32:15.6 and its epicentre is 9km from the closest station - FROB, see Figure 2b. Our NetCP model detects the first change-point at FROB with a high probability (≈ 0.78) at 22:32:17.35, a delay of 1.75 seconds. It is known² that P-waves travel fastest in the earths crust, at around 5-7 km/s. Thus, the expected time taken for the P-waves to reach FROB is between 1.29 - 1.8 seconds, consistent with the time of the first change-point under our model. Similarly, the furthest station, SMNB, is located 20.8km from the first epicentre and our model detects the first change-point here at 22:32:19.05, a delay of 3.45 seconds. Again, this is consistent with the expected time of arrival for P-waves (between 2.97 - 4.16 seconds). These delays agree with the inferred posterior graph structure displayed in Figure 2, which indicates that change-points propagate away from the epicentres.

¹<https://ncedc.org/ncedc/catalog-search.html>

²See for example: www.bgs.ac.uk/discovering-geology/earth-hazards/earthquakes/how-are-earthquakes-detected/

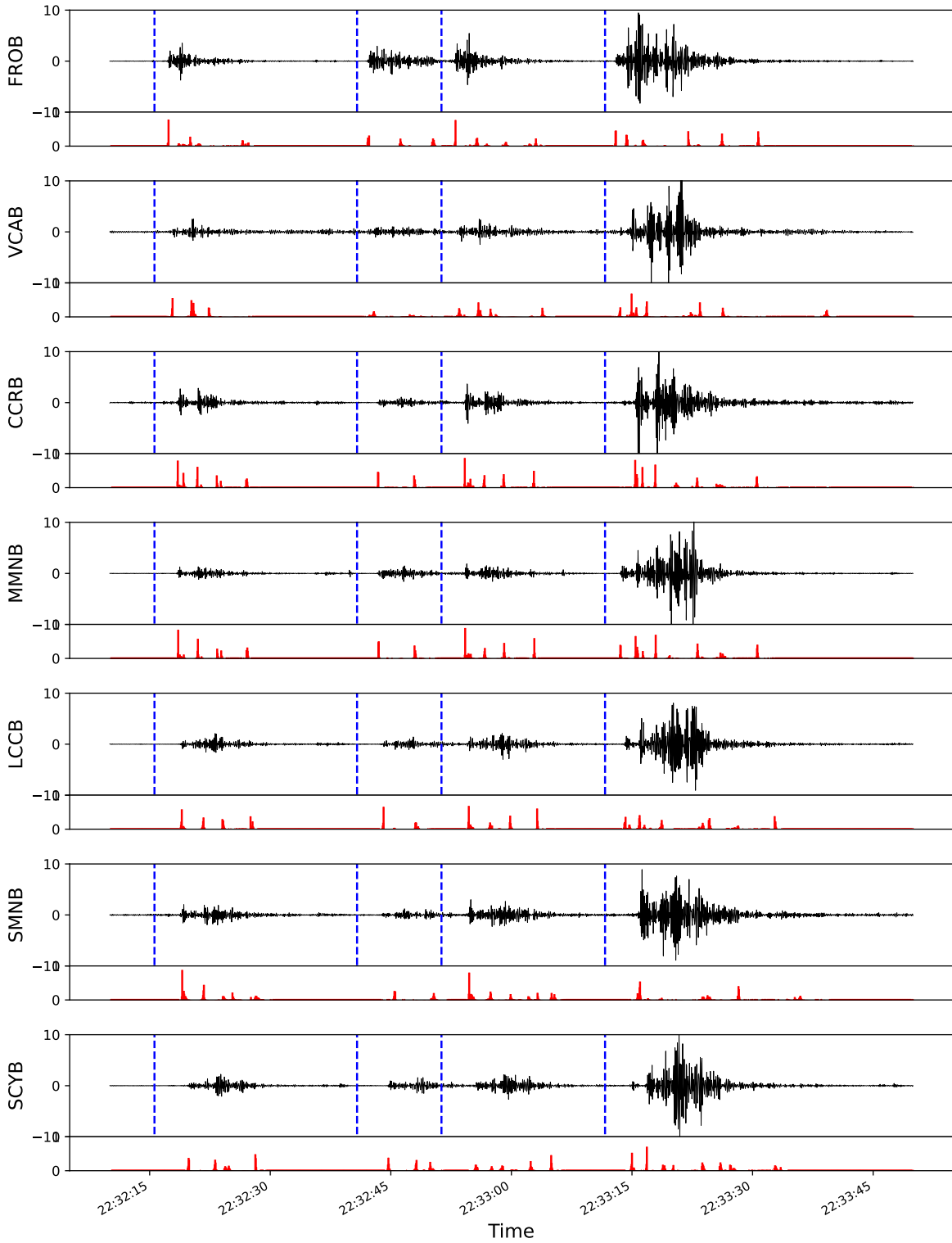


Figure 3: Processed signals (top) and estimated posterior change-point probabilities (bottom) under the proposed model for the seven geophone recording stations. Blue dashed lines indicate the recorded start times for the four microearthquakes.

4.3 EEG Data

We now apply our model to EEG signals collected from paediatric epilepsy patients at Boston Children’s Hospital. An EEG is a medical test which measures the electrical activity of the brain using electrodes

placed on the scalp, and is a key tool for diagnosing and monitoring epilepsy. These recordings provide important information about the onset, origin, and spread of seizures across brain regions. Change-point analysis may be used to uncover such information. For example, change-points may first appear in the signals from the temporal lobe electrodes before propagating to signals from frontal electrodes shortly after.

The data was obtained from the CHB-MIT Scalp EEG Database (Guttag, 2010) and was originally analysed by Shoeb (1981). We consider EEG data from patient CHB01, recorded during session 21. The raw signals are represented as bipolar montages, calculated as the voltage difference between pairs of adjacent electrodes in order to reduce noise. Temporal Lobe Epilepsy, characterized by seizures originating in the temporal lobes, is one of the most common forms of focal epilepsy in children. Based on this, we limit our analysis to six bipolar montages derived from eight electrodes placed in the temporal and frontal regions, see Figure 4. We focus on a 15 second segment of data from 325 to 340 seconds, during which a seizure is clinically annotated to begin at 327 seconds.

Before we proceed to analysing the EEG data, we preprocess it by applying a 1-30 Hz Butterworth bandpass filter in order to isolate the relevant frequency components (Chung et al., 2024). The signals, originally sampled at 256 Hz, are then downsampled by a factor of 3. We then apply first-order differencing and normalise each series to have zero mean and unit variance. The processed dataset then consists of $d = 6$ time series, each containing $T = 1279$ observations. We then use the same AR likelihood model and hyperparameter settings as in Section 4.2 and again ran two MCMC chains for 20,000 iterations with 200 particles and a burn-in of 2000.

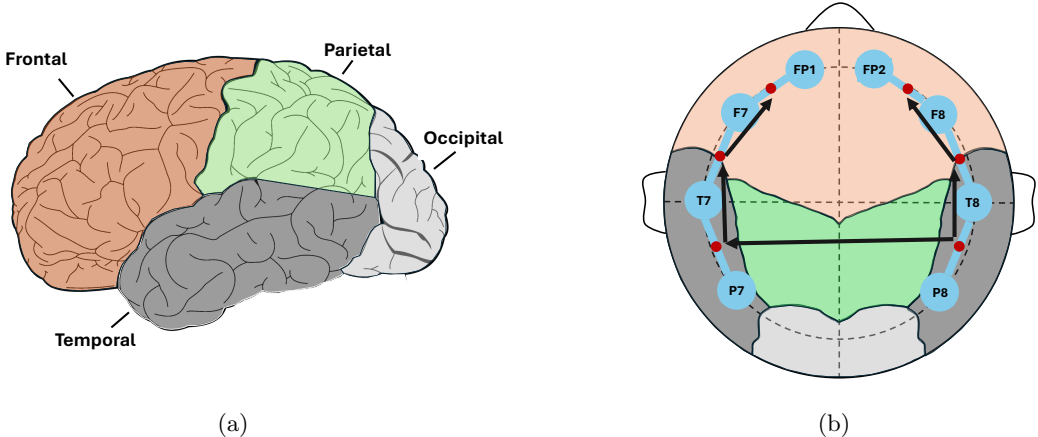


Figure 4: EEG Electrode Positions: (a) Labelled brain lobes coloured by region. (b) Top down view of electrode locations with colours corresponding to those in (a). Blue circles represent electrode locations. Blue edge with red dots indicate the bipolar montages that make up the raw signals. Black arrows indicate the edges obtained after thresholding $Pr(A_{i,j} = 1|\mathbf{y})$ at 50%.

Figure 5 displays the processed EEG signals and posterior change-point probabilities. The first change-point appears in the T8-P8 signal, and is consistent with the clinically annotated seizure start time. Subsequent change-points can be seen in all or subsets of the signals as the seizure activity continues to evolve and propagate to other regions of the brain.

Figure 4a displays the four brain lobes while Figure 4b displays the locations of the electrodes and bipolar montages which make up the six signals. Figure 4b displays the edges obtained after thresholding the posterior edge inclusion probabilities $Pr(A_{i,j} = 1|\mathbf{y})$ at 50%. The edges suggest that change-points are first observed in the right temporal lobes (electrodes T8/P8) before spreading to the left temporal lobe (electrodes T7/P7) and to the frontal lobes (electrodes FP1, FP2, F7, F8) shortly after. This suggests that the seizure originated in the region of the P8 electrode and is consistent with previous analysis by Chung et al. (2024), where the EEG signals were visually analysed by two neurologists. Although this dataset does not include diagnostic information about the patient, the observed propagation pathway in Figure 4a aligns with patterns commonly associated with Temporal Lobe Epilepsy (see Jacobs et al., 2008). Our analysis also supports the concept of epileptogenic networks, where seizures develop and propagate through localised brain networks rather than appearing

as isolated events (see Bartolomei et al., 2025).

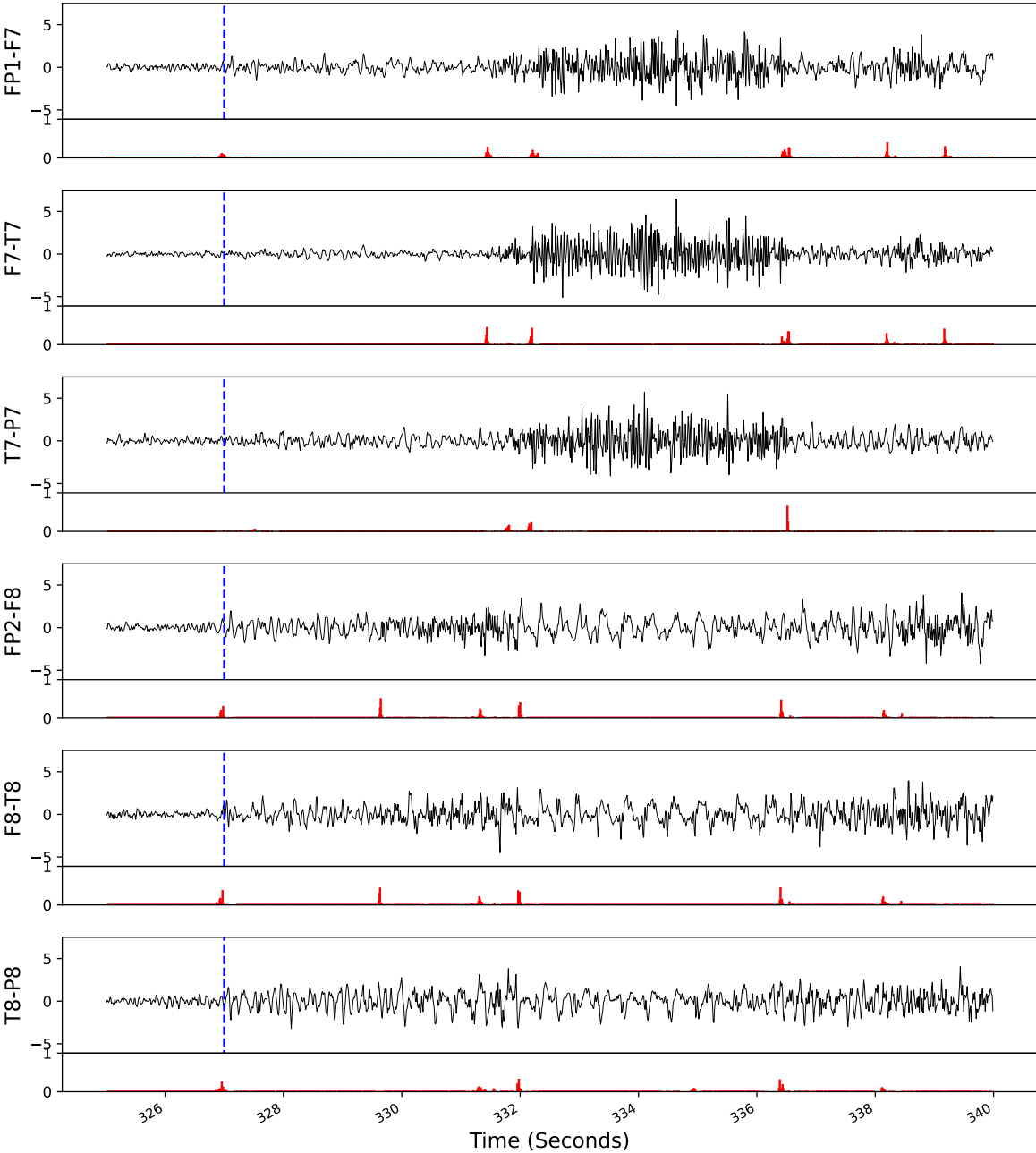


Figure 5: Processed EEG signals (top) and estimated posterior change-point probabilities (bottom) under the proposed model for the six bipolar montages. Blue dashed lines indicate the clinically annotated seizure onset time.

5 Discussion

In this work, we introduced a Bayesian framework for detecting change-points across multiple time series, specifically tailored to settings where subsets of series exhibit lead-lag relationships in their change-point locations. These dependencies are captured through a latent directed graph, where edge weights encode both the strength and delay of influence from leading to lagging series. Posterior inference is made tractable by extending efficient particle MCMC techniques originally developed for univariate change-point models.

Empirical results show that the proposed method outperforms existing approaches in scenarios with strong inter-series dependence in change-point structure. Moreover, the model successfully recovers interpretable latent network structures in real-world seismological and EEG datasets, providing a principled and automated way to detect and quantify lead-lag behaviour previously observed in these domains.

Although the MCMC algorithm employed performs well for the problems considered, scalability remains a challenge. The discrete and multimodal nature of the posterior poses difficulties for efficient sampling, and the computational cost scales linearly with the number of series, as a separate particle filter must be run for each. This highlights the need for more scalable inference methods in high-dimensional settings.

The proposed model may also be extended in several ways. A central assumption is that observations within a segment are independent of those in other segments. However, in many practical settings, this assumption may be overly restrictive—for example, when certain data characteristics persist or evolve gradually across segment boundaries. An extension to incorporate Markov switching dynamics, where segment-specific parameters can transition between a set of recurring states, may provide a more flexible framework for modelling data exhibiting distinct and recurring *regimes*. Similarly, the latent directed graph is assumed to be fixed. Future work may relax this to allow the graph to change at certain times, reflecting a shift in the lead-lag relationships.

Acknowledgements

Carson McKee was supported by the Heilbronn Institute for Mathematical Research. Data for this study come from the High Resolution Seismic Network (HRSN) doi:10.7932/HRSN, operated by the UC Berkeley Seismological Laboratory, which is archived at the Northern California Earthquake Data Center (NCEDC), doi: 10.7932/NCEDC. The simulation study was aided by the King’s Computational Research, Engineering and Technology Environment (CREATE) computing cluster.

Appendix A: Detailed MCMC Steps

Sampling Hidden States \mathbf{x}

Sampling the hidden states in series j , $\mathbf{x}_{j,0:T}$ using algorithm 1 requires additional algorithms to perform resampling and backward sampling. Since we are performing conditional particle filtering within a particle Gibbs framework, the previously sampled hidden states for series j are guaranteed to survive all resampling steps when filtering. We therefore use the conditional SOR algorithm described by algorithm 2. All of the below algorithms can be found in (Whiteley et al., 2011; Fearnhead and Liu, 2007).

Algorithm 2 Conditional Stratified Optimal Resampling

Require: $(\mathcal{S}_t, \mathcal{W}_t)$ particles/weights to resample, $x_{j,t}^*$ (current hidden state), N (number particles to keep).

- 1: Find κ such that $\sum_{s \in \mathcal{S}_t} \min(w_t(s)/\kappa, 1) = N$.
 - 2: For each $s \in \mathcal{S}_t$, if $w_t(s) > \kappa$, place particle s into set A . Otherwise place s into set B .
 - 3: Let $(\mathcal{S}_t^A, \mathcal{W}_t^A)$ and $(\mathcal{S}_t^B, \mathcal{W}_t^B)$ be the particles & weights for sets A and B respectively.
 - 4: Assume there are K particles in \mathcal{S}_t^A .
 - 5: **if** $x_{j,t}^* \in \mathcal{S}_t^B$ **then**
 - 6: Sample $N - K$ particles from $(\mathcal{S}_t^B, \mathcal{W}_t^B)$ using the Conditional Stratified Resampling Algorithm (conditional on $x_{j,t}^*$).
 - 7: **else**
 - 8: Sample $N - K$ particles from $(\mathcal{S}_t^B, \mathcal{W}_t^B)$ using the Stratified Resampling Algorithm.
 - 9: **end if**
 - 10: The surviving particles then consist of those from \mathcal{S}_t^A (with their original weights) and those that survived resampling from \mathcal{S}_t^B , each assigned weight κ .
-

Resampling the particles of set B in steps 6 and 8 requires either the conditional stratified resampling or stratified resampling algorithms. These are described by algorithm 3 and algorithm 4.

Algorithm 3 Conditional Stratified Resampling

Require: $(\mathcal{S}_t^B, \mathcal{W}_t^B)$ particles/weights to resample, $x_{j,t}^*$ (current hidden state), $N - K$ (number particles to keep).

- 1: Normalise the weights, \mathcal{W}_t^B , such that $\sum_{s \in \mathcal{S}_t^B} w_t^B(s) = 1$.
- 2: Construct the distribution function:

$$Q_t(s) = \sum_{\{s' \in \mathcal{S}_t^B: s' \leq s\}} w_t(s')$$

- 3: Sample V^* uniformly on $[Q_t(x_{j,t}^* - 1), Q_t(x_{j,t}^*)]$, set $V_1 = V^* - \frac{\lfloor (N-K)V^* \rfloor}{N-K}$ and $V_p = V_{p-1} + 1/(N-K)$ for $p = 2, \dots, N - K$.
 - 4: A particle $s \in \mathcal{S}_t^B$ survives resampling if there exists a V_p s.t. $Q_t(s - 1) \leq V_p \leq Q_t(s)$.
-

Algorithm 4 Stratified Resampling

Require: $(\mathcal{S}_t^B, \mathcal{W}_t^B)$ particles/weights to resample, $N - K$ (number particles to resample).

- 1: Normalise the weights, \mathcal{W}_t^B , such that $\sum_{s \in \mathcal{S}_t^B} w_t^B(s) = 1$.
- 2: Construct the cumulative distribution function:

$$Q_t(s) = \sum_{\{s' \in \mathcal{S}_t^B: s' \leq s\}} w_t^B(s')$$

- 3: Sample V_1 uniformly on $[0, 1/(N - K)]$ and set $V_p = V_{p-1} + 1/(N - K)$ for $p = 2, \dots, N - K$.
 - 4: A particle $s \in \mathcal{S}_t^B$ survives resampling if there exists a V_p s.t. $Q_t(s - 1) \leq V_p \leq Q_t(s)$.
-

After generating the particle approximations for each time $t = 1, \dots, T$, we generate a new sample $\mathbf{x}_{j,0:T}$ using backward sampling given in Algorithm 5.

Algorithm 5 Backward Sampling

Require: $\{(\mathcal{S}_t, \mathcal{W}_t)\}_{t=1, \dots, T}$ particle/weight sets after performing particle filtering on series j , \mathbf{x}^* (current matrix of hidden states).

- 1: Sample $x_{j,T}$ from the distribution on \mathcal{S}_T defined by the weights \mathcal{W}_T .
 - 2: **for** $t = T - 1, \dots, 1$ **do**
 - 3: Sample $x_{j,t}$ from the distribution on \mathcal{S}_t proportional to $w_t(x_{j,t})P_{t+1}^{(j)}(x_{j,t+1}|x_{j,t}, \mathbf{x}_{(-j),0:T}^*)$
 - 4: **end for**
 - 5: Return the sampled sequence $\mathbf{x}_{j,0:T} = (x_{j,t}, \dots, x_{j,T})$.
-

Sampling \mathbf{A}

We sample \mathbf{A} by Gibbs sampling each pair $(A_{i,j}, A_{j,i})$ for $i = 1, \dots, d, j = i + 1, \dots, d$. The full posterior conditional for each pair $(A_{i,j}, A_{j,i})$ is proportional to:

$$\pi(A_{i,j} = a_{i,j}, A_{j,i} = a_{j,i} | \mathbf{y}, \dots) \tag{35}$$

$$\propto Pr(A_{i,j} = a_{i,j}, A_{j,i} = a_{j,i} | \rho) Pr(\mathbf{x}_{i,0:T} | \mathbf{W}_0, \mathbf{W}, \mathbf{A}^*, \mathbf{q}_0, \mathbf{q}) Pr(\mathbf{x}_{j,0:T} | \mathbf{W}_0, \mathbf{W}, \mathbf{A}^*, \mathbf{q}_0, \mathbf{q}) \tag{36}$$

$$= Pr(A_{i,j} = a_{i,j}, A_{j,i} = a_{j,i} | \rho) \tag{37}$$

$$\times \prod_{t=1}^t Pr(X_{i,t} = x_{i,t} | \mathbf{X}_{t-1} = \mathbf{x}_{t-1}, \mathbf{W}_0, \mathbf{W}, \mathbf{A}^*, \mathbf{q}_0, \mathbf{q}) Pr(X_{j,t} = x_{j,t} | \mathbf{X}_{t-1} = \mathbf{x}_{t-1}, \mathbf{W}_0, \mathbf{W}, \mathbf{A}^*, \mathbf{q}_0, \mathbf{q}) \tag{38}$$

defined for $(a_{i,j}, a_{j,i}) \in \{(1, 0), (0, 1), (0, 0)\}$ and \mathbf{A}^* is the current adjacency matrix with the $a_{i,j}$ and $a_{j,i}$ imputed at (i, j) and (j, i) respectively. Thus, $(A_{i,j}, A_{j,i})$ can be updated using a categorical sample.

Sampling ρ

The full posterior conditional of ρ is given by

$$\pi(\rho|\cdots) \propto Pr(\mathbf{A}|\rho)f(\rho) \quad (39)$$

$$= (\rho/2)^{n_1}(1-\rho)^{n_2}\mathbf{1}(0 < \rho < 0.2) \quad (40)$$

where $n_1 = \sum_{i=1}^d \sum_{j=i+1}^d \mathbf{1}(A_{i,j} = 1 \cup A_{j,i} = 1)$ and $n_2 = \sum_{i=1}^d \sum_{j=i+1}^d \mathbf{1}(A_{i,j} = 0 \cap A_{j,i} = 0)$. This is a $Beta(1 + n_1, 1 + n_2)$ distribution truncated on the interval $(0, 0.2)$ and may be sampled using rejection sampling.

Sampling $(\mathbf{W}_0, \mathbf{W}, \mathbf{q}_0, \mathbf{q})$

Due to correlation between $(W_{i,j}, q_{i,j})$, we find that it is beneficial to update these jointly for $j = 1, \dots, d$; $i = 0, \dots, d$. We update $(W_{i,j}, q_{i,j})$ with a random walk Metropolis step using independent Gaussian proposals: $W_{i,j}^\dagger \sim \mathcal{N}(W_{i,j}, 0.5^2)$ and $q_{i,j}^\dagger \sim \mathcal{N}(q_{i,j}, 0.05^2)$. We then accept $(W_{i,j}^\dagger, q_{i,j}^\dagger)$ with probability

$$\frac{Pr(\mathbf{X} = \mathbf{x}|W_{i,j}^\dagger, q_{i,j}^\dagger, \cdots)Ga(W_{i,j}^\dagger|1, 1)I(0 < q_{i,j}^\dagger < 1)}{Pr(\mathbf{X} = \mathbf{x}|W_{i,j}, q_{i,j}, \cdots)Ga(W_{i,j}|1, 1)I(0 < q_{i,j} < 1)}$$

In practice, we find that thinning the above Metropolis update by around 15 steps produces good mixing in the datasets considered.

Appendix B: Comparison of Gibbs Sampling Schemes

Here we provide a comparison of the particle Gibbs scheme presented in Section 3 and the ‘‘single-site’’ Gibbs sampler which samples each $X_{j,t}$ one at a time from their full posterior conditionals. We simulate data with $d = 4$ series and $T = 1000$ time points from scenario **S1** with the Gaussian means likelihood model from Section 4.1. The simulated data can be seen in Figure 6. We then estimated the NetCP model using the same hyperparameters given in Section 4.1 using (i) single-site Gibbs (SSG), (ii) particle Gibbs with 50 particles (PG50) and (iii) particle Gibbs with 100 particles (PG100). For each sampler we generated 20,000 posterior samples, discarding the first 2000 as burn-in.

The estimated marginal posterior change-point probabilities for series one under each sampling method are shown in Figure 7. We can see that the estimated probabilities for each method are virtually identical. In order to assess the mixing properties of the methods, we may inspect the sampled hidden states at each iteration. From Figure 7 we can see that in series one, time point 583 has around 0.6 probability of being included as a change-point. We can assess the mixing of $X_{1,583}$ by inspecting the sampled values of $U_{1,583} = I(X_{1,583} = 582)$. I.e. $U_{1,583} = 1$ for a change-point and $U_{1,583} = 0$ for no change-point.

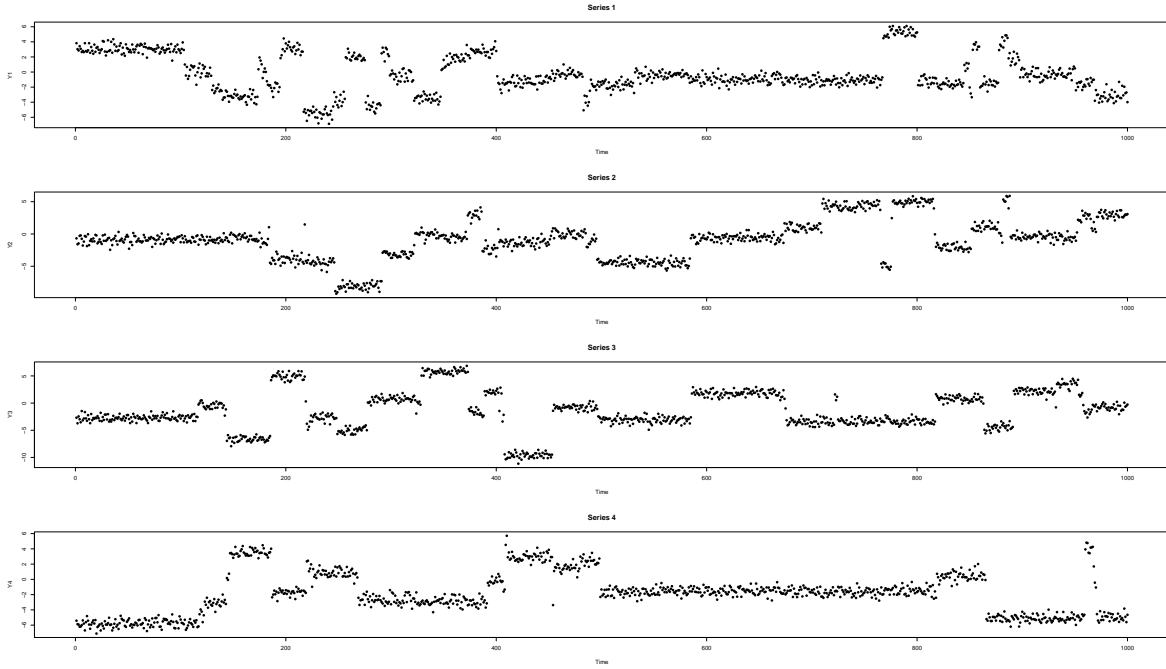


Figure 6: Simulated Times Series

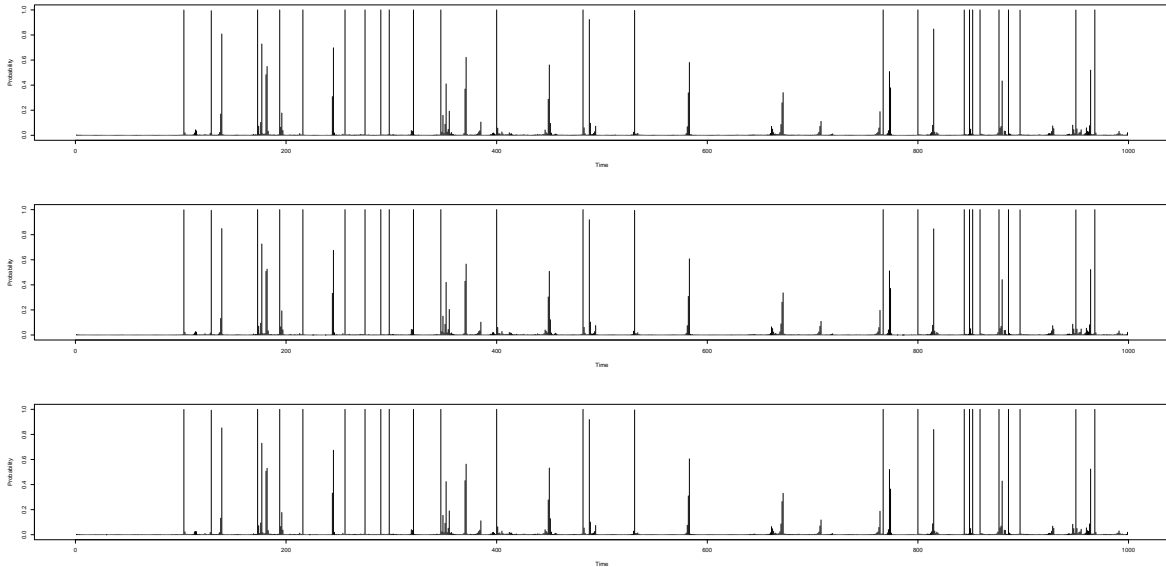


Figure 7: Estimated marginal posterior change-point probabilities for series one using SSG (top), PG50 (middle) and PG100 (bottom).

From Figure 8 we can see that under the single-site Gibbs sampler, $U_{1,583}$ mixes very poorly, getting stuck in a given state for long periods of time. However, the particle Gibbs methods with 50 and 100 particles both appear to be mixing much better. This is evident in the autocorrelation plots in Figure 8. Here the single-site Gibbs exhibits a slow decay in the correlation between samples while the particle Gibbs samples decorrelate almost immediately. We then estimated the integrated autocorrelation time (IAT) of each method using the R function (“IAT”). The single-site Gibbs obtains an IAT of 58.5 while the particle Gibbs schemes both obtain IATs of 1.2. This suggests that we must obtain around 49 samples from the single-site sampler in order to obtain the same amount of information as one sample from particle Gibbs samplers (when estimating $\mathbb{E}[U_{1,583}|\mathbf{y}]$). Similar results can be obtained by

inspecting the change-point indicators at other time points. These results suggest that relatively few particles are required to achieve good mixing, with the particle Gibbs sampler obtaining the same IAT for 50 and 100 particles.

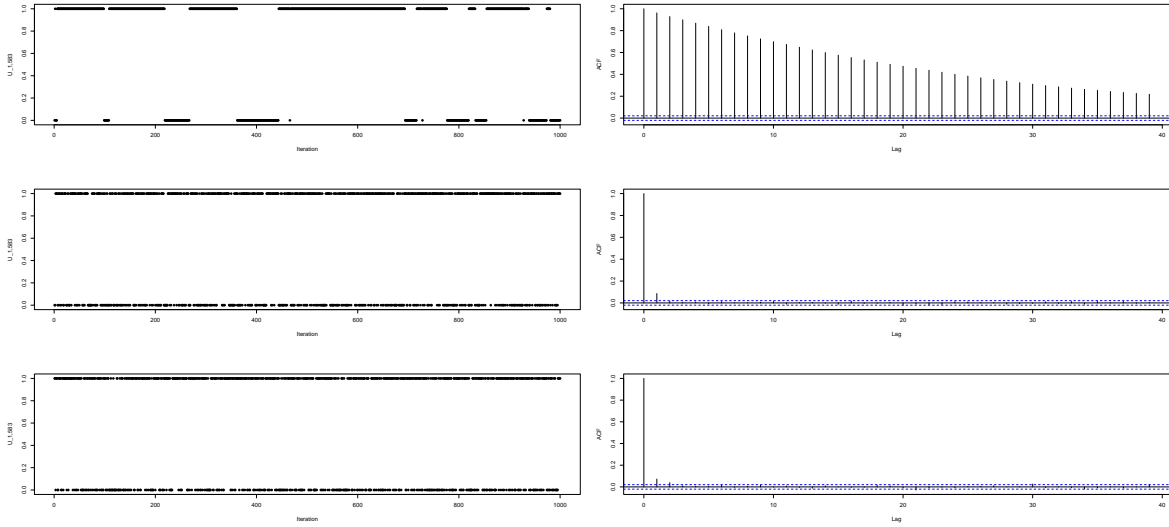


Figure 8: First 1000 samples after burn-in (left column) and estimated autocorrelation function (right column) of $U_{1,583}$ for SSG (top row), PG50 (middle row) and PG100 (bottom row).

Appendix C: Marginal Segment Likelihood for Gaussian Mean Model

Under the Gaussian changing means likelihood model considered in Section 4.1, the likelihood for a given segment $s : t$ in series j is given by

$$f_j(\mathbf{y}_{j,s:t}|\theta) = \prod_{k=s+1}^t \mathcal{N}(y_{j,k}|\theta, \sigma_j^2)$$

and the prior on θ is given by $f_j(\theta) = \mathcal{N}(\theta|0, \gamma_j^2)$. Upon integrating over θ within each segment, we obtain the marginal segment density

$$f_j(\mathbf{y}_{j,s:t}) = \frac{1}{(2\pi\sigma_j^2)^{(t-s)/2}} \left(\frac{\sigma_j^2}{(t-s)\gamma_j^2 + \sigma_j^2} \right)^{1/2} \exp \left(-\frac{\sum_{k=s+1}^t y_{j,k}^2}{2\sigma_j^2} + \frac{\gamma_j^2 \left[\sum_{k=s+1}^t y_{j,k} \right]^2}{2\sigma_j^2 \left((t-s)\gamma_j^2 + \sigma_j^2 \right)} \right)$$

which depends on the hyperparameters (σ_j^2, γ_j^2) .

References

- Alaya, M. A. B., Ternynck, C., Dabo-Niang, S., Chebana, F., and Ouarda, T. B. (2020). Change point detection of flood events using a functional data framework. *Advances in Water Resources*, 137:103522.
- Andrieu, C., Doucet, A., and Holenstein, R. (2010). Particle markov chain monte carlo methods. *Journal of the Royal Statistical Society: Series B (Statistical Methodology)*, 72:269–342.
- Bardwell, L. and Fearnhead, P. (2017). Bayesian detection of abnormal segments in multiple time series. *Bayesian Analysis*, 12:193–218.

- Barry, D. and Hartigan, J. A. (1992). Product partition models for change point problems. *The Annals of Statistics*, 20:260 – 279.
- Barry, D. and Hartigan, J. A. (1993). A bayesian analysis for change point problems. *Journal of the American Statistical Association*, 88:309.
- Bartolomei, F., Makhalova, J., Benoit, J., and Lagarde, S. (2025). The different subtypes of temporal lobe seizures networks. *Revue Neurologique*, 181:368–381.
- Bauwens, L., Carpentier, J. F., and Dufays, A. (2017). Autoregressive moving average infinite hidden markov-switching models. *Journal of Business & Economic Statistics*, 35:162–182.
- Beal, M. J., Ghahramani, Z., and Rasmussen, C. E. (2002). The infinite hidden markov model. In *Proceedings of the 15th International Conference on Neural Information Processing Systems: Natural and Synthetic*, NIPS’01, page 577–584.
- Caudron, C., White, R. S., Green, R. G., Woods, J., Ágústsdóttir, T., Donaldson, C., Greenfield, T., Rivalta, E., and Brandsdóttir, B. (2018). Seismic amplitude ratio analysis of the 2014–2015 bór arbunga-holuhraun dike propagation and eruption. *Journal of Geophysical Research: Solid Earth*, 123:264–276.
- Chernoff, H. and Zacks, S. (1964). Estimating the current mean of a normal distribution which is subjected to changes in time. *The Annals of Mathematical Statistics*, 35(3):999–1018.
- Chib, S. (1996). Calculating posterior distributions and modal estimates in markov mixture models. *Journal of Econometrics*, 75(1):79–97.
- Chib, S. (1998). Estimation and comparison of multiple change-point models. *Journal of Econometrics*, 86:221–241.
- Chopin, N. (2006). Dynamic detection of change points in long time series. *Annals of the Institute of Statistical Mathematics 2006 59:2*, 59:349–366.
- Chung, Y. G., Cho, A., Kim, H., and Kim, K. J. (2024). Single-channel seizure detection with clinical confirmation of seizure locations using chb-mit dataset. *Frontiers in Neurology*, 15:1389731.
- Corradin, R., Danese, L., and Ongaro, A. (2022). Bayesian nonparametric change point detection for multivariate time series with missing observations. *International Journal of Approximate Reasoning*, 143:26–43.
- Erdős, P. and Rényi, A. (1959). On random graphs. i. *Publicationes Mathematicae*, 6:290–297.
- Fan, Z. and Mackey, L. (2017). Empirical bayesian analysis of simultaneous changepoints in multiple data sequences. *Annals of Applied Statistics*, 11:2200–2221.
- Fearnhead, P. (2006). Exact and efficient bayesian inference for multiple changepoint problems. *Statistics and Computing*, 16:203–213.
- Fearnhead, P. and Clifford, P. (2003). On-line inference for hidden markov models via particle filters. *Journal of the Royal Statistical Society: Series B (Statistical Methodology)*, 65(4):887–899.
- Fearnhead, P. and Liu, Z. (2007). On-line inference for multiple changepoint problems. *Journal of the Royal Statistical Society: Series B (Statistical Methodology)*, 69:589–605.
- Fryzlewicz, P. (2014). Wild binary segmentation for multiple change-point detection. *Annals of Statistics*, 42:2243–2281.
- García, E. C. and and, E. G.-P. (2019). Nonparametric product partition models for multiple change-points analysis. *Communications in Statistics - Simulation and Computation*, 48(7):1922–1947.
- Green, P. J. (1995). Reversible jump markov chain monte carlo computation and bayesian model determination. *Biometrika*, 82:711.
- Guttag, J. (2010). *CHB-MIT Scalp EEG Database (version 1.0.0)*, *PhysioNet*.

- Hallgren, K. L., Heard, N. A., and Turcotte, M. J. (2024). Change-point detection on a graph of time series. *Bayesian Analysis*, 19:649–676.
- Hartigan, J. A. (1990). Partition models. *Communications in Statistics - Theory and Methods*, 19:2745–2756.
- Jacobs, J., Dubeau, F., Olivier, A., and Andermann, F. (2008). Pathways of seizure propagation from the temporal to the occipital lobe. *Epileptic Disorders*, 10:266–270.
- Jeng, X. J., Cai, T. T., and Li, H. (2013). Simultaneous discovery of rare and common segment variants. *Biometrika*, 100:157–172.
- Kass-Hout, T. A., Xu, Z., McMurray, P., Park, S., Buckeridge, D. L., Brownstein, J. S., Finelli, L., and Groseclose, S. L. (2012). Application of change point analysis to daily influenza-like illness emergency department visits. *Journal of the American Medical Informatics Association*, 19:1075–1081.
- Killick, R., Fearnhead, P., and Eckley, I. A. (2012). Optimal detection of change-points with a linear computational cost. *Journal of the American Statistical Association*, 107:1590–1598.
- Liu, S., Wright, A., and Hauskrecht, M. (2017). Change-point detection method for clinical decision support system rule monitoring. *Artificial intelligence in medicine. Conference on Artificial Intelligence in Medicine (2005-)*, 10259:126.
- Maheu, J. M. and Song, Y. (2018). An efficient bayesian approach to multiple structural change in multivariate time series. *Journal of Applied Econometrics*, 33:251–270.
- NCEDC (2014). *Northern California Earthquake Data Center, UC Berkeley Seismological Laboratory*.
- Nyamundanda, G., Hegarty, A., and Hayes, K. (2015). Product partition latent variable model for multiple change-point detection in multivariate data. *Journal of Applied Statistics*, 42:2321–2334.
- Page, E. S. (1954). Continuous inspection schemes. *Biometrika*, 41:100–115.
- Quinlan, J. J., Page, G. L., and Castro, L. M. (2024). Joint random partition models for multivariate change point analysis. *Bayesian Analysis*, 19:21–48.
- Shoeb, A. H. (1981). Application of machine learning to epileptic seizure onset detection and treatment. *PhD Thesis, Harvard-MIT Division of Health Sciences and Technology*.
- Siegmund, D., Yakir, B., and Zhang, N. R. (2011). Detecting simultaneous variant intervals in aligned sequences. *The Annals of Applied Statistics*, 5:645–668.
- Truong, C., Oudre, L., and Vayatis, N. (2020). Selective review of offline change point detection methods. *Signal Processing*, 167:107299.
- Wang, T. and Samworth, R. J. (2018). High dimensional change point estimation via sparse projection. *Journal of the Royal Statistical Society Series B: Statistical Methodology*, 80:57–83.
- Whiteley, N., Andrieu, C., and Doucet, A. (2011). Bayesian computational methods for inference in multiple change-points models. *Technical Report, University of Bristol*.
- Xie, L., Xie, Y., and Moustakides, G. V. (2019). Asynchronous multi-sensor change-point detection for seismic tremors. *IEEE International Symposium on Information Theory - Proceedings*, 2019-July:2199–2203.
- Yao, Y.-C. (1984). Estimation of a noisy discrete-time step function: Bayes and empirical bayes approaches. *The Annals of Statistics*, 12:1434–1447.
- Zhang, N. R., Siegmund, D. O., Ji, H., and Li, J. Z. (2010). Detecting simultaneous change-points in multiple sequences. *Biometrika*, 97:631–645.